

cy. 2



# VELOCITY DETERMINATION BY MEASUREMENT OF THE DOPPLER SHIFT OF A SPECTRAL LINE

H. T. Bentley, III, V. A. Cline, and E. D. Tidwell

ARO, Inc.

April 1972

Approved for public release; distribution unlimited.

**ARNOLD ENGINEERING DEVELOPMENT CENTER  
AIR FORCE SYSTEMS COMMAND  
ARNOLD AIR FORCE STATION, TENNESSEE**

# *NOTICES*

When U. S. Government drawings specifications, or other data are used for any purpose other than a definitely related Government procurement operation, the Government thereby incurs no responsibility nor any obligation whatsoever, and the fact that the Government may have formulated, furnished, or in any way supplied the said drawings, specifications, or other data, is not to be regarded by implication or otherwise, or in any manner licensing the holder or any other person or corporation, or conveying any rights or permission to manufacture, use, or sell any patented invention that may in any way be related thereto.

Qualified users may obtain copies of this report from the Defense Documentation Center.

References to named commercial products in this report are not to be considered in any sense as an endorsement of the product by the United States Air Force or the Government.

VELOCITY DETERMINATION BY MEASUREMENT  
OF THE DOPPLER SHIFT  
OF A SPECTRAL LINE

H. T. Bentley, III, V. A. Cline, and E. D. Tidwell  
ARO, Inc.

Approved for public release; distribution unlimited.

## FOREWORD

The research reported herein was sponsored by the Arnold Engineering Development Center (AEDC), Air Force Systems Command (AFSC), under Program Element 64719F.

The results reported herein were obtained by ARO, Inc. (a subsidiary of Sverdrup & Parcel and Associates, Inc.), contract operator of AEDC, AFSC, Arnold Air Force Station, Tennessee, under Contract F40600-72-C-0003. The research was performed from July 1969 to July 1970 under ARO Project BB5027, and the manuscript was submitted for publication on May 24, 1971.

The authors wish to acknowledge the guidance and technical assistance of H. J. Ramm. They further wish to acknowledge R. T. Schneider of the University of Florida for his help in the adaptation of the rotating refractor plate.

This technical report has been reviewed and is approved.

David G. Francis  
Captain, USAF  
Research and Development  
Division  
Directorate of Technology

Robert O. Dietz  
Acting Director  
Directorate of Technology

**ABSTRACT**

Measurement of gas velocity in a high enthalpy, arc-heated facility has usually been inferentially derived. The ability to measure a directly related quantity, the shift in frequency of an emitting spectral line, enables the velocity to be obtained in a noninteracting manner. The theory concerning the line shape and other inversion requirements is discussed. Three mathematical techniques for separating the lines are discussed and examples of each are given. Furthermore, the results of an Abel inversion are obtained. The test apparatus which consists of the high velocity arc source, optics, spectrometer, and either a photographic plate or electro-optical readout is described, and experimental results are presented. Velocity measurements obtained by the various experimental and mathematical techniques are compared as to accuracy, speed, and ease of data reduction.

## CONTENTS

	<u>Page</u>
ABSTRACT . . . . .	iii
NOMENCLATURE . . . . .	vi
I. INTRODUCTION . . . . .	1
II. THEORY . . . . .	1
III. EQUIPMENT . . . . .	15
IV. PHOTOELECTRIC SCANNING . . . . .	23
V. DATA ACQUISITION . . . . .	27
VI. DATA REDUCTION . . . . .	28
VII. SUMMARY . . . . .	34
REFERENCES . . . . .	38
APPENDIX: Computerized Form of Abel Inversion . . . . .	39

## ILLUSTRATIONS

Figure

1. Schematic of Optics . . . . .	3
2. Gaussian Curve Fit . . . . .	5
3. Distortion of Composite Line . . . . .	6
4. Abel Inversion . . . . .	8
5. Input Data . . . . .	10
6. Inverted Data . . . . .	10
7. Plot of $\alpha$ versus Normalized Doppler Shift . . . . .	12
8. Plot of $\beta$ versus Normalized Doppler Shift . . . . .	13
9. Plot of $\gamma$ versus Normalized Doppler Shift . . . . .	14
10. Arc Accelerator . . . . .	16
11. Arc Facility . . . . .	18
12. Relative Intensity of the 4266 Å Ar II Level versus Time . . . . .	19
13. Photoelectric Scanning . . . . .	24
14. Refractor Plate . . . . .	25
15. Electronics Schematic . . . . .	26

<u>Figure</u>	<u>Page</u>
16. Shifted Argon Lines . . . . .	31
17. Iron Calibration Lines . . . . .	31
18. Abel Inversion with Intensity Monitor, Input Data . . .	35
19. Abel Inversion with Intensity Monitor, Inverted Data . .	36
20. Comparison of Input and Inverted Data at Peak Intensities . . . . .	37

**TABLES**

I. Photographic Plate Identification . . . . .	29
II. Test Results of Photoelectric Technique . . . . .	32
III. Test Results of Photographic Technique . . . . .	33

**NOMENCLATURE**

A	Area matrix
a	Area
c	Speed of light
e	Electronic charge
I	Intensity matrix
$\hat{I}$	Inverted intensity matrix
I	Intensity
k	Boltzman's constant
m	Electron mass
R	Radius of plume
r	Radius
T	Temperature, °K
V	Velocity, m/sec
$\gamma'$	Natural line width
$\delta$	Halfwidth at half maximum intensity

$\theta$	Viewing angle
$\lambda$	Wavelength, Å
$\nu$	Frequency, Hz

**SUBSCRIPTS**

c	Composite
D	Doppler
i	Station
j	Radius
o	Unshifted, or integrated
s	Single
1	Upstream
2	Downstream

## SECTION I INTRODUCTION

During the early 1960's much emphasis was placed on the development of electric arc thrusters and magnetohydrodynamic devices for use as space thrusters. Simultaneously, similar devices were developed for use in wind tunnel applications; i. e., reentry, satellite and solar wind simulators. Most of these devices produced environments hostile to the use of aerodynamic probe techniques. For example, high heat-transfer rates require extensive cooling of most probes. Aerodynamic measurement of enthalpy by means of mass sampling techniques are severely handicapped by transitional flow effects. Similar problems also exist for pitot pressure probes.

Although integrated measurements of introduced mass flow, thrust, and energy balance could be obtained, the average velocity could not. This fundamental measurement could not be obtained directly from the thrust equation because of the large entrained mass flow values (Ref. 1). For these reasons, a noninterfering method was sought.

The purpose of the study reported here was, therefore, to determine the most promising method by which a routinely applicable velocity measuring device could be based. The purpose of this report is to summarize the approaches taken and to make a critical comparison of different techniques to show the direction in which a final development of such a device will have to go.

## SECTION II THEORY

Measurement of the Doppler shift of a spectral emission line requires a knowledge of the line profile. The following sections discuss these effects. The modification of spectral lines attributable to instrumental broadening, although admittedly important, has not been included. Further work, which includes inversion of the observed lines, should take these effects into consideration.

## 2.1 DOPPLER SHIFT AND LINE SHAPE

The apparent change in wavelength of radiation caused by a velocity difference between the radiation source and observer is given by

$$\lambda_0 - \lambda' = \lambda_0 V/c$$

Where  $V$  is taken to be positive when the source is moving toward the observer,  $\lambda_0$  is the unshifted wavelength, and  $\lambda'$  is the shifted wavelength. This shift can be experimentally obtained by observing the radiation from two different optical paths through the luminous flow as in Fig. 1. For a uniform flow velocity  $V$ , the shift in wavelength between the two lines is

$$\lambda_D = \lambda_1' - \lambda_2' = \lambda_0 \frac{V}{c} (\cos \theta_1 + \cos \theta_2)$$

Again the primed symbols indicate the wavelength of the shifted lines. (For clarity, incremental symbols have been dropped from  $\lambda_D$ .) Although any combination of angles could be chosen, they were made as nearly equal as possible to minimize effects caused by axially dependent variation in velocity or intensity. Of course, the angle should be minimized to maximize the measurable shift and thereby improve accuracy.

Spectra were recorded either directly on photographic plates or on an oscilloscope after first being detected by a photomultiplier tube and scanning device. In either case, it was possible to record the radiation from both lines in two ways: either simultaneously, which resulted in an unresolved composite line, or at two different times which lead to distinct lines (Section 2.3).

When the lines are distinct, an average velocity can be obtained by measuring the relative peak displacement with little regard for the line shape. However, for unresolved lines, the shape of the composite line, when compared to that of a single distinct line, contains the Doppler shift information.

The line shape for dipole radiation of a single spectral line is given by the classically derivable Lorentzian line profile when written in terms of frequency

$$I(\nu) = \frac{\gamma'}{2\pi} \frac{I_0}{4\pi^2(\nu_0 - \nu)^2 + \left(\frac{\gamma'}{2}\right)^2}$$

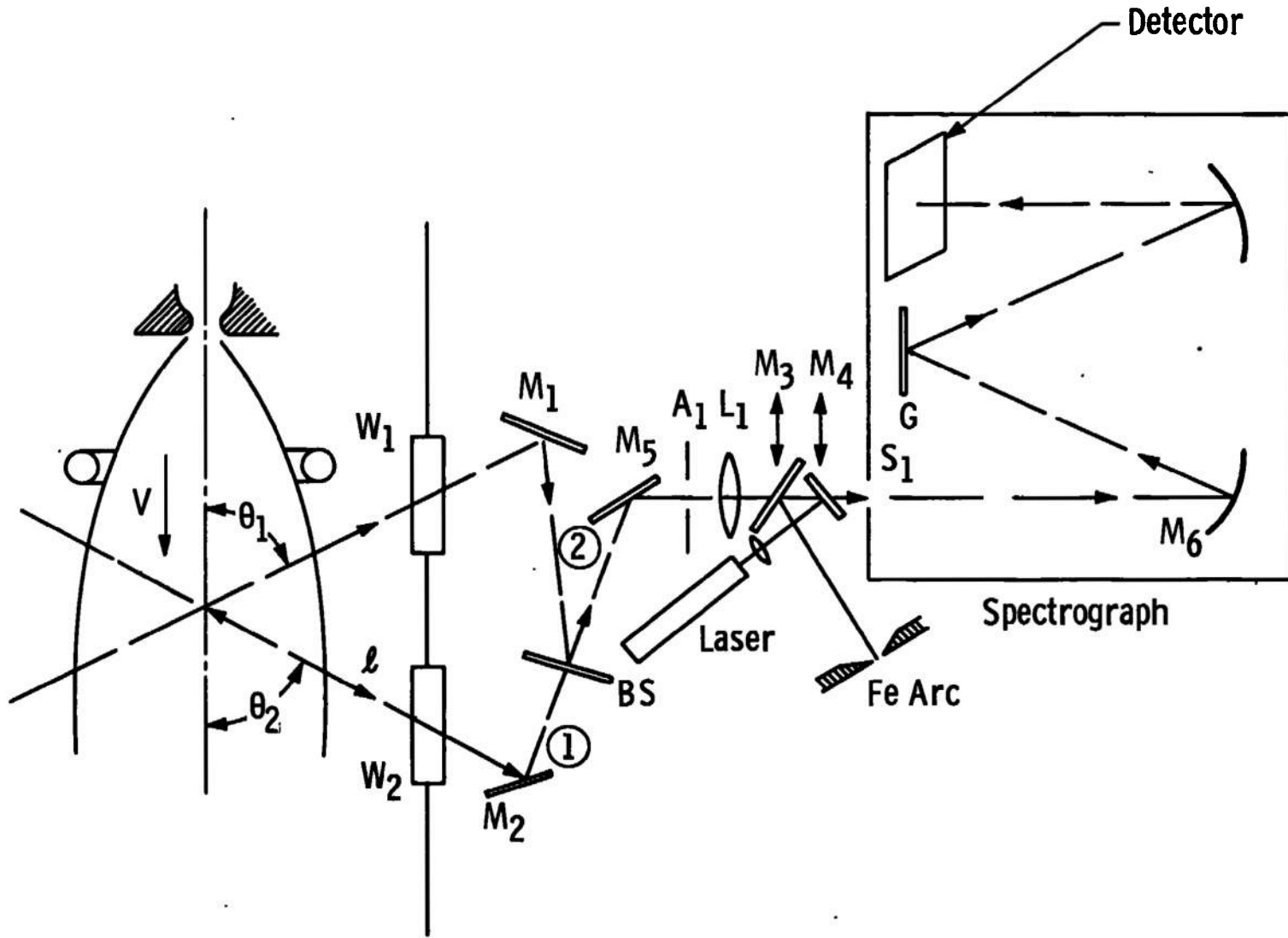


Fig. 1 Schematic of Optics

where

$$\gamma' = \frac{8\pi^2 e^2 \nu_0^2}{3mc^3} \text{ (cgs units); } I_0 = \int_{\text{all } \nu} I(\nu) d\nu$$

The natural line width is characteristically small:  $1.16 \times 10^{-4} \text{ \AA}$ . However, in the case of thermally energetic gases the thermal motion can broaden line radiation into the Doppler profile which is Gaussian. The relative intensity as a function of frequency is

$$I(\nu) = I_0 e^{-\frac{mc^2}{2kT} \left(1 - \frac{\nu_0}{\nu}\right)^2}$$

The full width at half of maximum intensity is

$$1.67 \frac{1}{\nu_0} \sqrt{\frac{2kT}{m}} = 1.67 \frac{\lambda_0}{c} \sqrt{\frac{2kT}{m}}$$

This relation is frequently used to determine the heavy particle temperature.

Figure 2 shows a Gaussian curve fit to the  $4266.53 \text{ \AA}$  Ar II line obtained by a photographic method and a photoelectrical method. Each has been arbitrarily normalized. The difference in their half-widths is attributable to instrumental broadening effects. In the photographic method the line was reduced from the plate by means of a microphotometer and strip-chart readout, whereas the photoelectric line was taken directly from an oscilloscope trace. The selection of an accurate base line is critical for certain methods as will be shown later. Actually, a Gaussian curve should not in general be a good fit as the line is a sum over the entire optical path. For example a skewed line can result even though the contributing effects are gaussian (Fig. 3). Of course, the flow properties are continuous rather than discrete, and it is the function of an inversion technique to include these effects.

## 2.2 ABEL INVERSION

The line intensity  $I(x)$  is related to the radial emission coefficient  $\hat{I}(r)$  in the usual manner by the relation (Refs. 3, 4, 5, and 6)

$$I(x) = 2 \int_x^R \frac{\hat{I}(r) r dr}{(r^2 - x^2)^{1/2}}$$

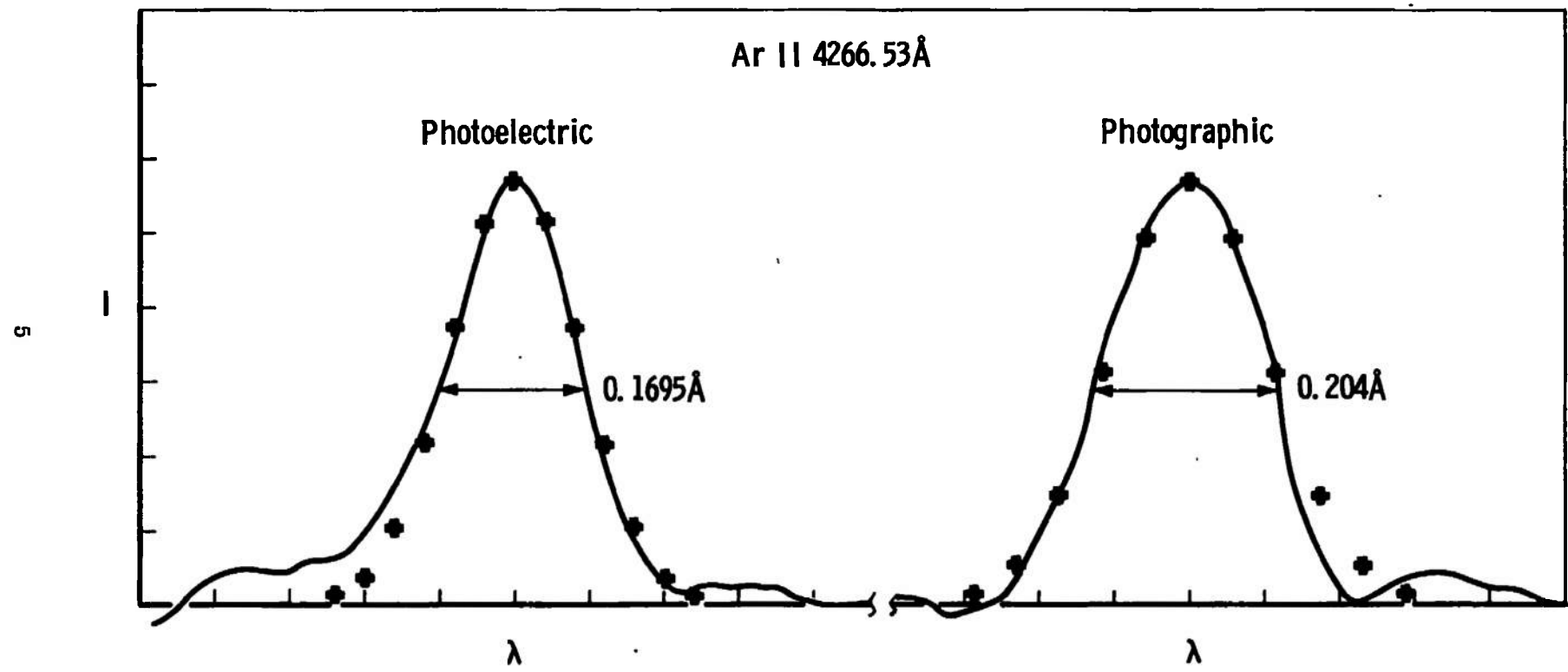


Fig. 2 Gaussian Curve Fit

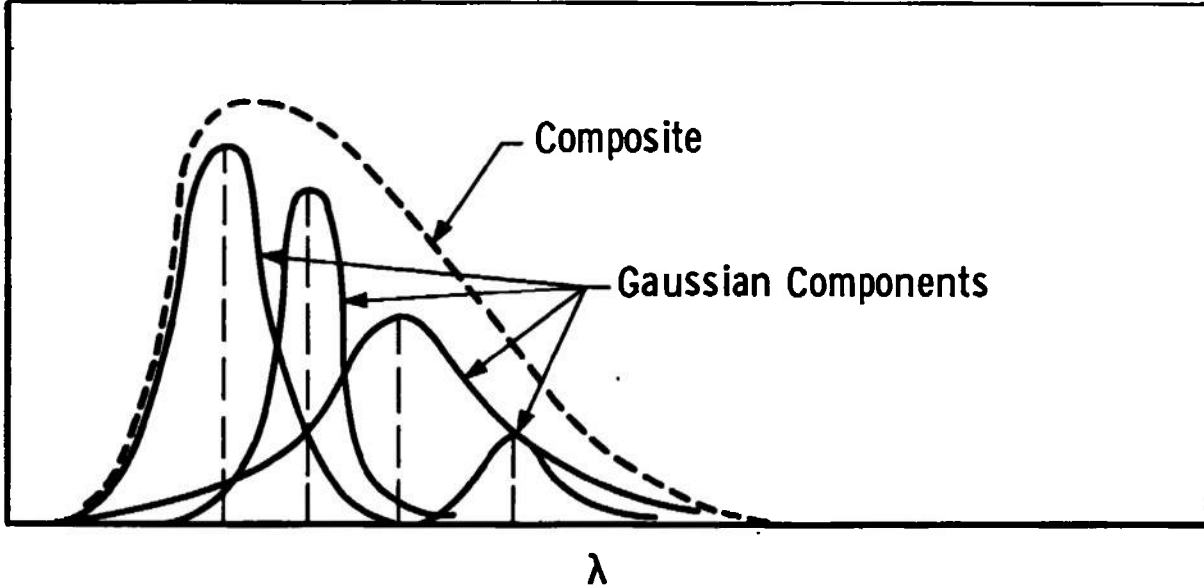


Fig. 3 Distortion of Composite Line

The inversion is given by

$$\hat{I}(r) = -\frac{1}{\pi} \int \frac{I'(x) dx}{r \cdot (x^2 - r^2)^{1/2}}$$

where  $I' = \frac{dI}{dx}$

However, in the case of finite station widths (Fig. 4) an incremental approach must be taken. The plume is considered to be composed of a series of concentric rings of unit spacing and unit depth. This assumption is valid even though the angle of view is not normal to the flow axis. The viewing angle increases the observed intensities,  $I(x)$ 's, by the multiplier  $\csc \theta$  for the cylindrically symmetric case. The intensity observed at station  $i$  is assumed to be a sum over all the rings contained in the slice, weighted by elemental areas. That is

$$I_i = \sum_{j=1}^{j=n} a_{i,j} \hat{I}_j$$

In matrix form

$$I = A \hat{I}$$

where

$$I = \begin{bmatrix} I_1 \\ I_2 \\ \vdots \\ I_n \end{bmatrix} \dots \hat{I} = \begin{bmatrix} \hat{I}_1 \\ \hat{I}_2 \\ \vdots \\ \hat{I}_n \end{bmatrix}$$

$$A = \begin{bmatrix} A_1 & | & A_2 & | & \dots & | & A_n \end{bmatrix}$$

The  $A$ 's which form the triangular matrix  $A$  are found in the Appendix.

To determine the radial distribution one simply forms  $\hat{I} = A^{-1}I$ . As  $A$  is triangular, a Gauss reduction can be performed yielding rather directly the  $\hat{I}$ 's.

Since only relative intensity was required, units were not rigidly adhered to. Any scaling was performed after inversion and was merely as a matter of convenience.

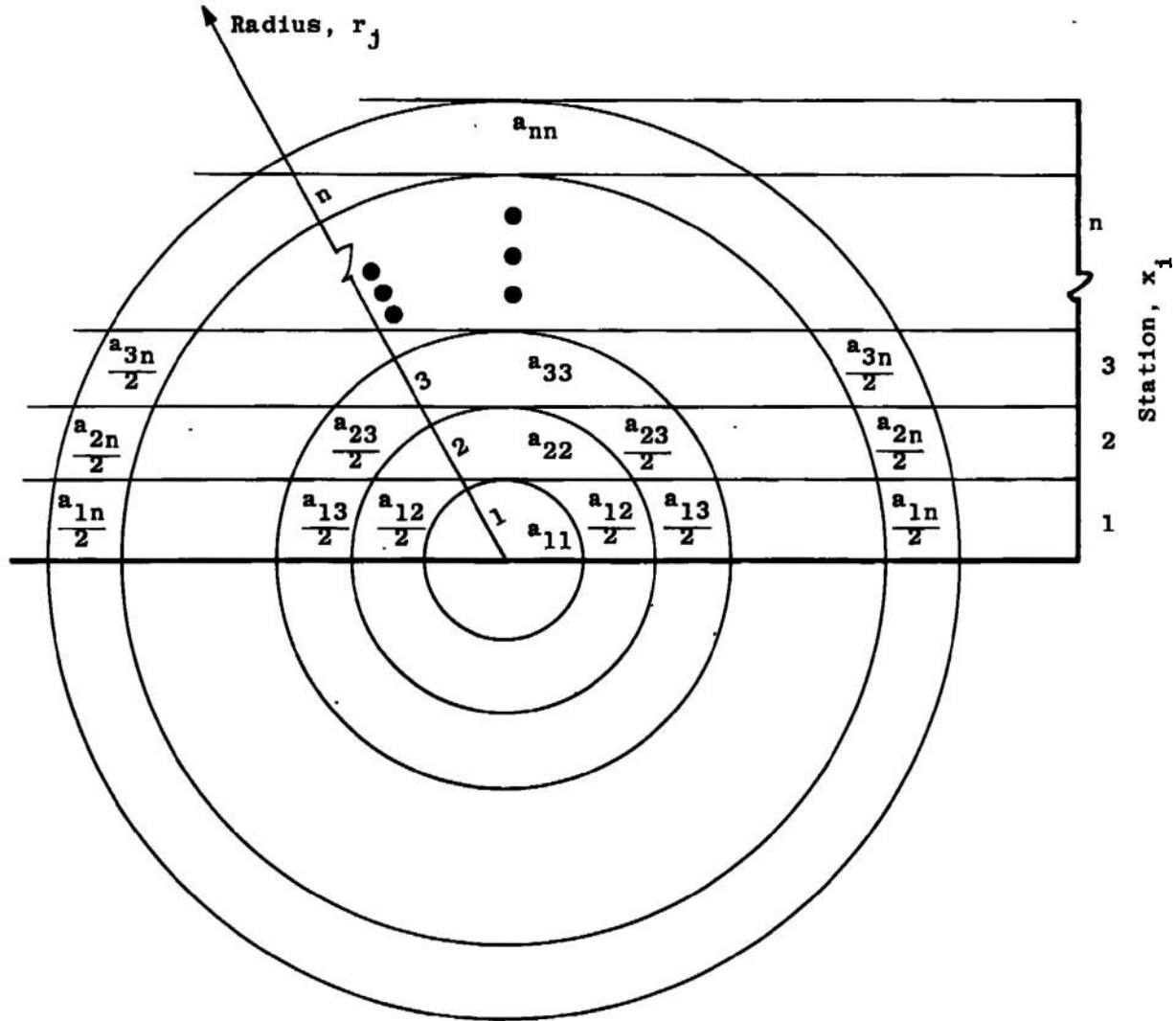


Fig. 4 Abel Inversion

Input data were composed of  $n$  profiles of  $I$  versus  $\lambda$  with  $\lambda_0$  corresponding to  $\lambda_D = 0$  obtained. This provided a three-dimensional array as shown in Fig. 5. The inversion program enters at a constant  $\lambda$  and inverts the data. The number of such inversions depends on the number of data points making up each input profile; the three-dimensional array of  $I$ ,  $r$ ,  $\lambda$  is formed (Fig. 6). These are the inverted data, and their treatment is described below.

### 2.3 DOPPLER SHIFT MEASUREMENTS

The measurement is either in the form of a composite unresolved line plus a single line or two distinct lines recorded at different times. The exact form determines the means of data reduction.

When the lines are distinct, measurements can be made in one of two ways:

1. If the two differently shifted lines can be independently superimposed, such as they could in a photoelectric recording, the measurement of the shift can be made directly by measuring the peak displacements.
2. When the two lines were on different spectra, as with the photographic plate, a reference system of lines from a standard source was superimposed. Measurements were then taken with respect to a nearby standard reference line. In both cases two reference lines are required to obtain the system dispersion.

When noise is a factor, whether caused by electronic or emulsion grain effects, several estimates of the location of the center can be made. The center of an intensity trace can be estimated several times by obtaining the midpoint of the full width at various fractions of the maximum line intensity. The center of a line viewed directly from the photographic plate, as with a contour projector, can be estimated by taking several measurements along the length of the line.

The Doppler shift can be obtained from the characteristics of a composite and single line shape. Three such techniques were developed, each requiring a different form of the data. As the algebraic manipulations are straightforward, only the general form and the results for a Gaussian line shape are shown.

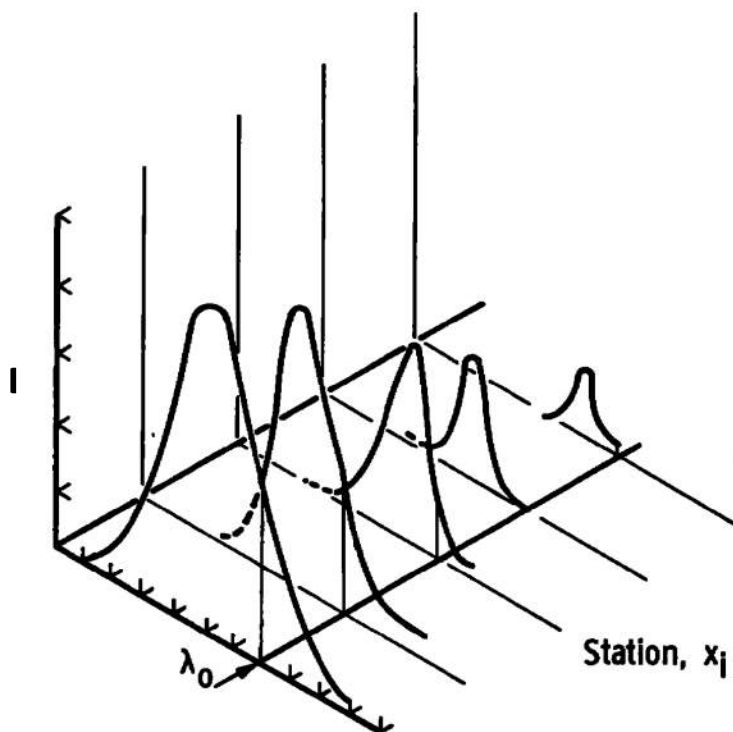


Fig. 5 Input Data

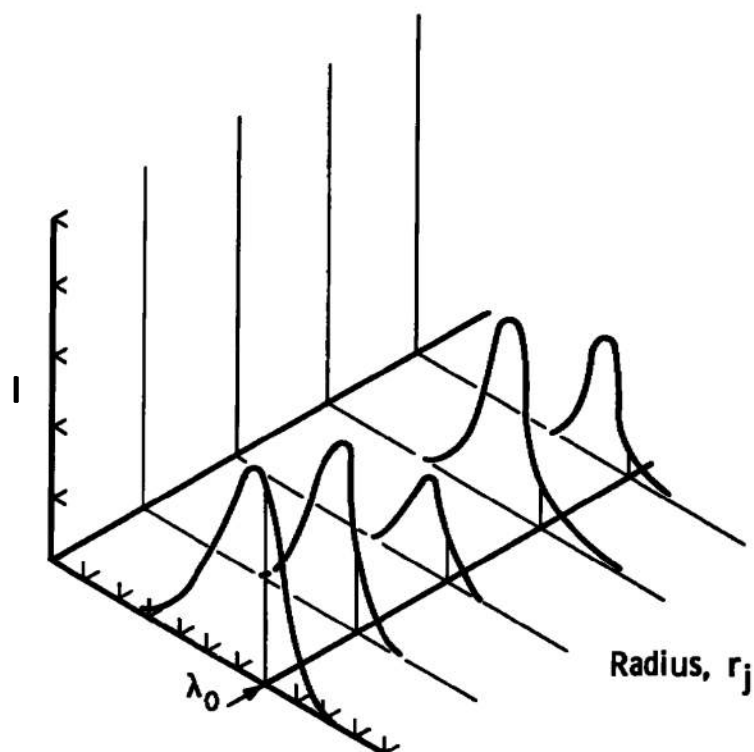


Fig. 6 Inverted Data

Most line profiles are given in the form  $I = I_0 f(\lambda - a)$  where  $(a)$  is assumed to be the center of the line and corresponds to that wavelength where  $I = I_0$ . The composite profile consists of the sum of two equal intensity profiles which are shifted from each other by an amount  $\lambda_D$ , the Doppler shift. If all measurements are made relative to the center of this line, then the composite profile is given by

$$I_c(\lambda) = I_0 \left[ f\left(\lambda + \frac{\lambda_D}{2}\right) + f\left(\lambda - \frac{\lambda_D}{2}\right) \right]$$

The first method uses a parameter  $\alpha$  which is the ratio of the composite line intensity evaluated at its center to that of a single line at its center; i. e.,

$$\alpha \equiv \frac{I_c(0)}{I_0} = f\left(-\frac{\lambda_D}{2}\right) + f\left(\frac{\lambda_D}{2}\right)$$

The Doppler shift for a Gaussian distribution, when normalized to the single line's half-width at one half maximum intensity,  $\delta_S$ , is

$$\frac{\lambda_D}{\delta_S} = 2 \left[ \frac{-\ln \frac{\alpha}{2}}{\ln 2} \right]^{1/2}$$

Figure 7 indicates that for large separations the method becomes very sensitive to small changes in intensity ratios. The main shortcoming of this method is that great care must be taken when exposures are made. A very slight imbalance attributable to exposure time, for example, can cause considerable error. The instrument as utilized could not readily achieve this criterion as all shutter operations were manually controlled.

The second method utilizes the parameter  $\beta$  which is the ratio of the intensity of the composite line, evaluated at  $\pm \delta_S$  from its center, to the composite's intensity at its center; i. e.,

$$\beta_{\pm} \equiv \frac{I_c(\pm \delta_S)}{I_c(0)} = \frac{f\left(\pm \delta_S + \frac{\lambda_D}{2}\right) + f\left(\pm \delta_S - \frac{\lambda_D}{2}\right)}{f\left(\frac{\lambda_D}{2}\right) + f\left(-\frac{\lambda_D}{2}\right)}$$

Again the Doppler shift for a Gaussian distribution is

$$\frac{\lambda_D}{\delta_S} = \frac{\ln \left( 2\beta \pm \sqrt{4\beta^2 - 1} \right)}{\ln 2}$$

This is shown plotted in Fig. 8. Since measurements are taken from a single line profile composite and the invariant half-width, exposure matching is not a problem.

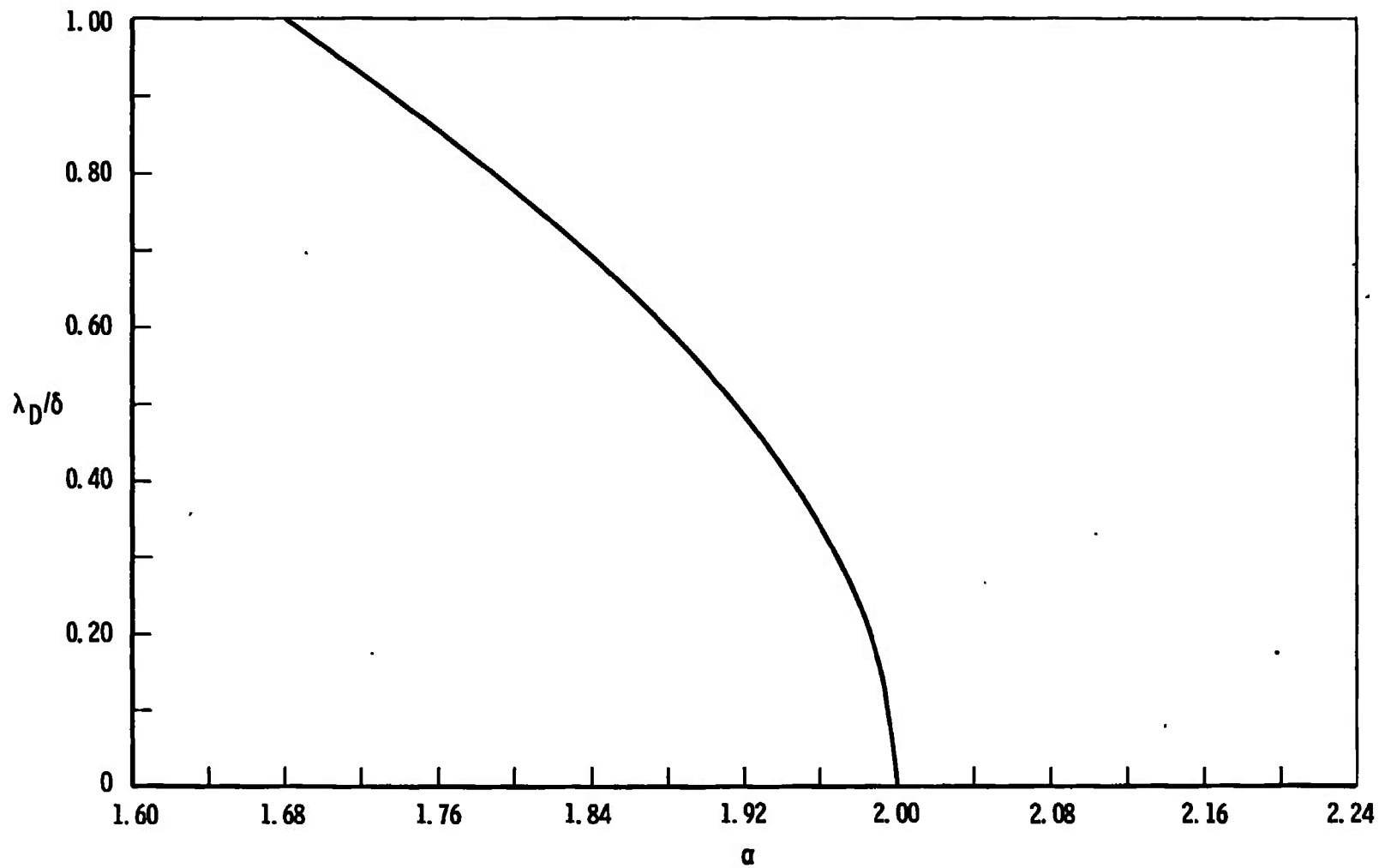


Fig. 7 Plot of  $\alpha$  versus Normalized Doppler Shift

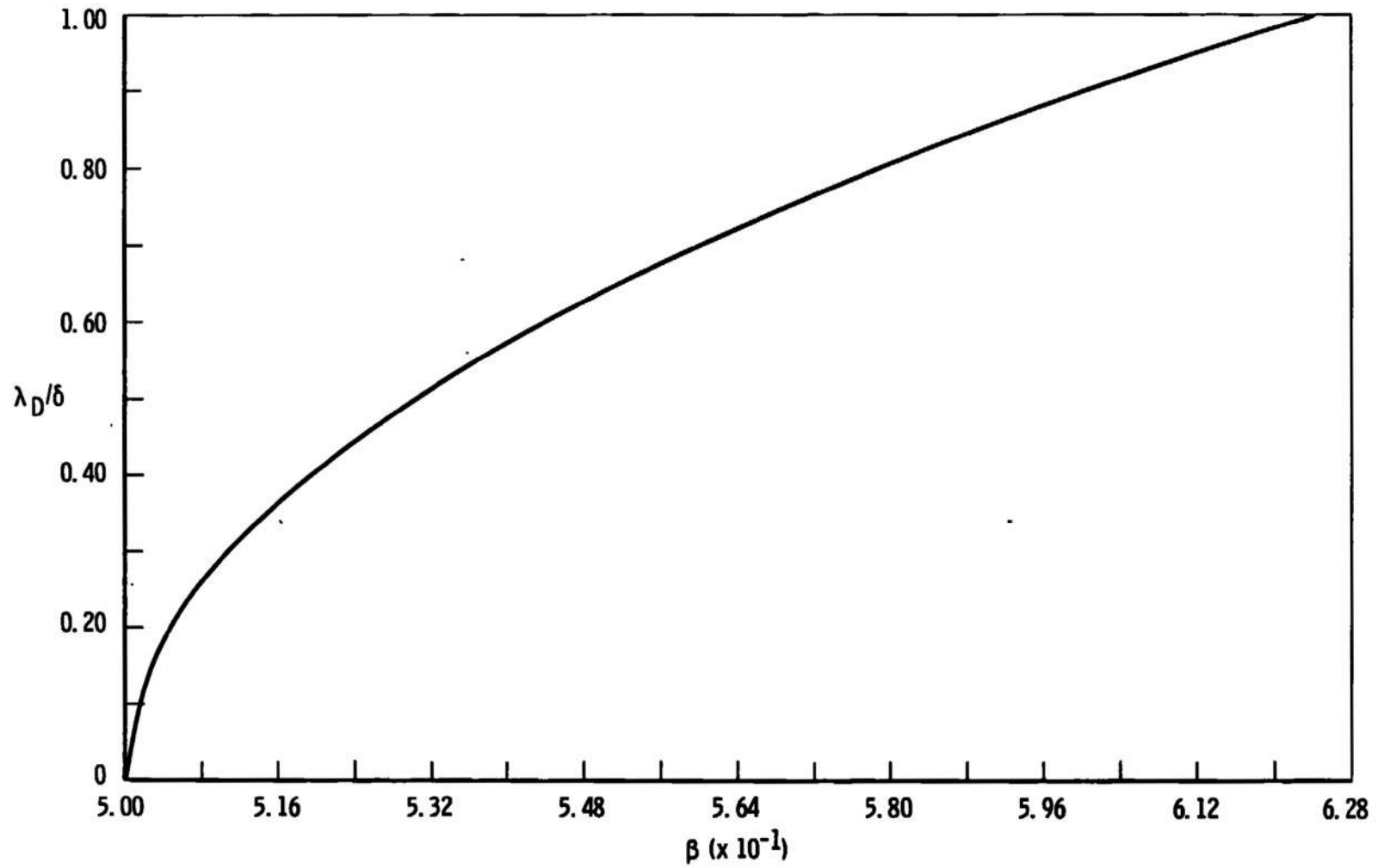


Fig. 8 Plot of  $\beta$  versus Normalized Doppler Shift

14

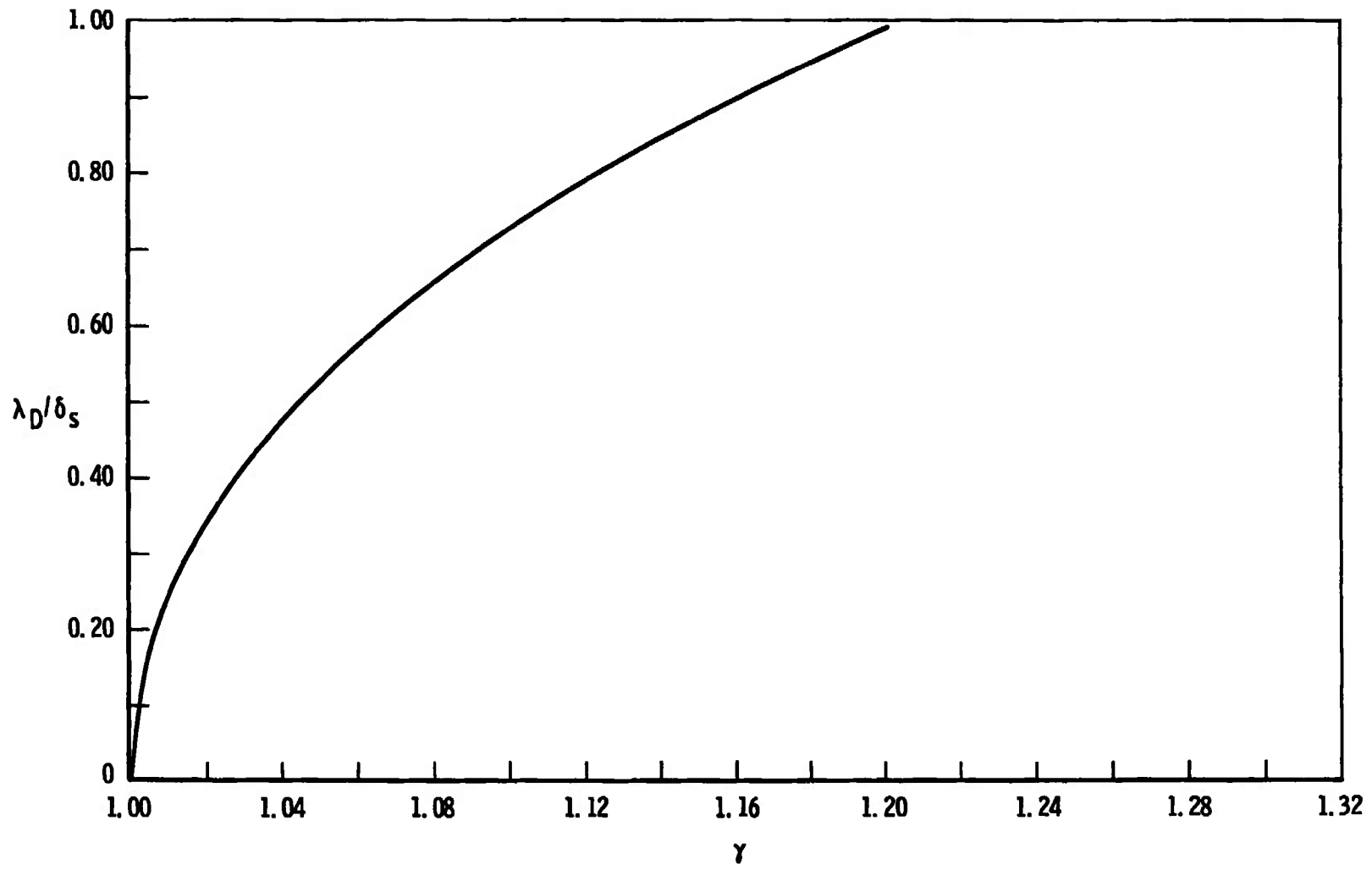


Fig. 9 Plot of  $\gamma$  versus Normalized Doppler Shift

The final method utilizes the ratio of the half-widths of a single and a composite line as measured at one half the center intensity. This ratio is

$$\gamma \equiv \frac{\delta_c}{\delta_s}$$

With no shift this ratio is unity and increases with increasing  $\lambda_D$ . This method requires only the measurement of the half-widths to obtain the shift and perhaps is the most straightforward approach.

The general implicit relation is

$$I_c(\pm \delta_c) = [I_c(0)]/2.$$

or

$$f\left(\pm \delta_c + \frac{\lambda_D}{2}\right) + f\left(\pm \delta_c - \frac{\lambda_D}{2}\right) = 1/2 \left[ f\left(\frac{\lambda_D}{2}\right) + f\left(-\frac{\lambda_D}{2}\right) \right]$$

For the Gaussian line shape (Fig. 9)

$$\frac{\lambda_D}{\delta_s} = \frac{\ln \left( \frac{\gamma^2 - 1}{2} \pm \sqrt{\frac{2(\gamma^2 - 1)}{2} - 1} \right)}{\gamma \ln 2}$$

### SECTION III EQUIPMENT

The apparatus consisted of the high velocity arc source, intermediate optics, a dispersion element in the form of a spectrometer, and either a photographic plate or a scanner and a photomultiplier tube. Photographic data reduction required a photodensitometer or a traveling microscope. When data were to be taken electronically, an oscilloscope triggered by the scanner was used to make photographic recordings of the data.

#### 3.1 HIGH VELOCITY ARC SOURCE

The tests were conducted using a self-magnetic arc accelerator. The electrodes for the d-c arc were configured to utilize the self-induced magnetic field of the discharge to accelerate the ionized argon working gas (Fig. 10). The current flows from the anode to the cathode,

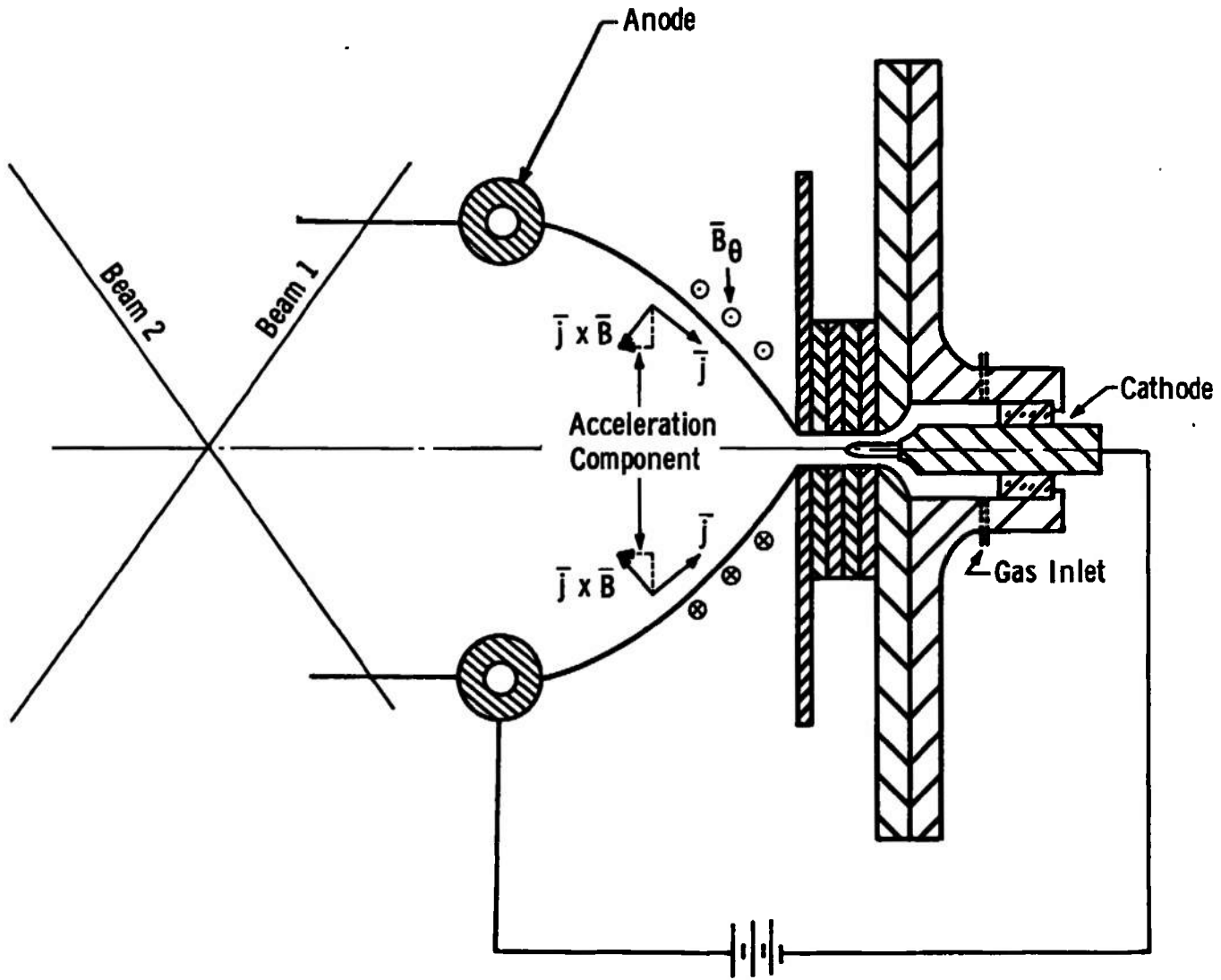


Fig. 10 Arc Accelerator

heating, ionizing and accelerating the gas as it expands. The plume is diffuse with no evidence of "spoke" formation. At the point of observation, just downstream of the anode ring, the plume was axisymmetric and about 6 in. in diameter.

The device was contained in a 4- by 4- by 8-ft vacuum chamber (Fig. 11). Optical access was provided by quartz windows in the test cell.

A combination of pumps was used to obtain typical test cell pressures of  $100 \mu\text{Hg}$ .

The arc power supply was current controlled and capable of supplying current up to 6000 amp. All data were taken at the following conditions:

Current	1500 amp
Voltage	53.5 volts
Working Gas	Argon
Mass Flow Rate	0.075 gm/sec

Although the arc parameters remained quite constant, the light intensity from a single spectral line decreased in time (Fig. 12). This phenomenon paralleled the heating of engine components and could be caused by quenching of metastable states by impurities. No effect was observed upon the velocity measured at different times into a run, utilizing the peak-peak shift method. Since data acquisition times were not coincident, a systematic error would result when other data reduction techniques were used, because intensity matching was important. To reduce this problem, data were taken about 60 sec after arc startup.

### 3.2 SPECTROMETER

A Jarrell Ash 1.5-m grating spectrometer Model 75-000 was used. To avoid vibration, the spectrometer was isolated from the test cell and pumps by a separate stand with foam rubber pads. Although small displacements could exist between the arc and the spectrograph because of the mounting arrangement, this effect was considered to be negligible. All optical components were mounted either directly to the spectrometer's optical bench or to a 0.5-in. -thick aluminum plate secured to it.

Slit width capabilities are from 4 to  $400 \mu$ , where the lower limit is controlled by an automatic stop to protect the edges. The practical lower limit, because of diffraction, is about  $10 \mu$ . To shorten required run

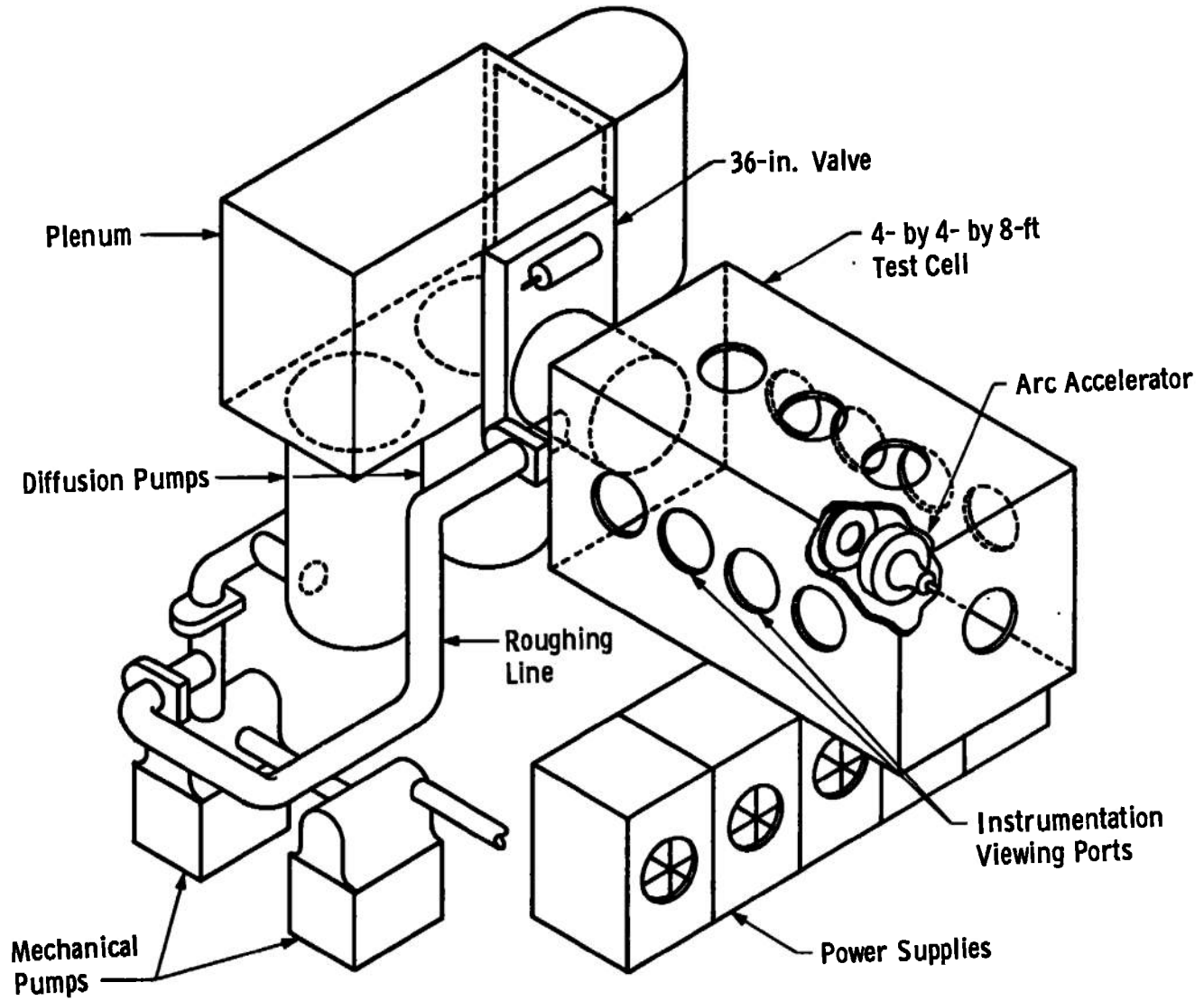


Fig. 11 Arc Facility

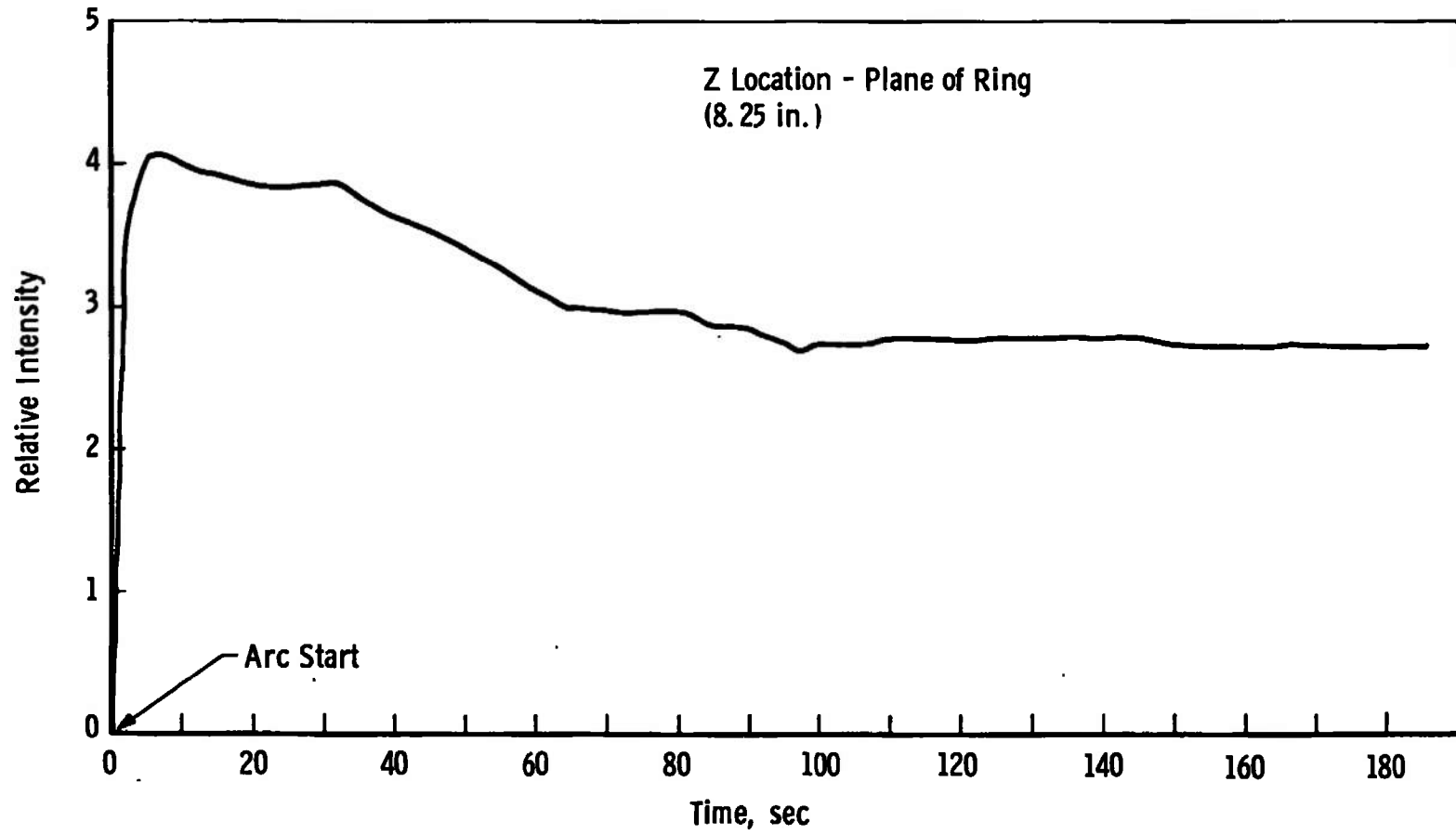


Fig. 12 Relative Intensity of the 4266Å Ar II Line versus Time

times the slit widths used were increased from 17 to 20  $\mu$ . This had little effect on the line widths; e. g., a 3- $\mu$  slit adjustment would increase a 0.20- $\text{\AA}$ -wide Ar II line to 0.215  $\text{\AA}$ . When scanning onto the phototube, a compromise was made between resolution and the signal-to-noise ratio. Slit height has only second-order effects on the resolution. A 3-mm height was used throughout the tests.

The spectrometer also had to be adjusted for maximum resolution. This was achieved by adjustments at both the entrance slit and the focal plane at the exit of the spectrometer by use of the iron arc source. Adjustments were first made for the photographic plate by a series of exposures at different entrance slit widths and plate angles. When this was finished, the photomultiplier assembly and the exit slit were inserted and optimized by adjusting the assembly and rotating the entrance slit. In this manner both the photographic and photoelectric assemblies were optimized and thereafter could be interchanged at will.

### 3.3 STANDARD SOURCE

A standard source for wavelength calibration was a Jarrell-Ash, Fe-Ne hollow cathode arc which had a maximum current of 20 ma. The d-c power supply was regulated and had a ripple factor of 0.05 percent. The source was mounted on the spectrometer where it could be focused on the entrance slit by means of a lens and a flip mirror.

### 3.4 INTERMEDIATE OPTICS

The purpose of the intermediate optics was to collect radiation from the plume along two predetermined paths, combine them in such a manner that they were collinear, and focus this radiation on the entrance slit of the spectrometer. Furthermore, symmetry conditions were to be maintained while the maximum possible velocity component was to be viewed.

The system functions as follows (Fig. 1). Light from the two paths passes through the windows  $W_1$  and  $W_2$  and is directed to the beam splitter, BS, by mirrors  $M_1$  and  $M_2$ . Here they are combined and directed through the aperture  $A_1$  and the lens L by the mirror  $M_5$ . The lens focuses the arc centerline image on the spectrometer entrance slit,  $S_1$ . Auxiliary movable mirrors  $M_3$  and  $M_4$  direct the iron arc and the helium-neon alignment laser, respectively.

All mirrors were front-surfaced and aluminum coated. The beam splitter was aluminized quartz with a nominal 40-percent transmission coefficient.

Aperture  $A_1$  serves primarily as a field stop to maintain an  $f$ /number of 12. This prevents overfilling the spectrometer focusing mirrors. The aperture was located as close to the lens as possible so that the relative weighting of the contributions along the optical path in the plume was unchanged by changes in aperture setting. When only one set of measurements was to be made, the system focused on the arc centerline rather than at infinity. This weighed all portions of the plume equally as the optical and plume geometries were nearly congruent.

### 3.4.1 Alignment

Alignment of the intermediate optics was achieved through the use of a laser and a target system. Mirror  $M_4$  was placed in front of the entrance slit and a removable, prealigned set of targets was placed on the optics bench. Minor adjustments of the laser and mirror provided a reference beam which was on the spectrometer optical axis. From this point adjustments were made working backward to the two mirrors  $M_1$  and  $M_2$ . Two very small pieces of reflective tape on the far test cell wall were used as targets to achieve this final alignment. Considerable care was taken to eliminate or minimize all other reflected light through blacking of the test cell surfaces. The results of improper precautions, where a corner reflector was inadvertently produced, are discussed later.

Rather than calculate the focal points for the lens, another lens was placed in front of the laser to focus the beam to a point. The distance from this point to mirror  $M_4$  was adjusted to coincide with that from the mirror to the entrance slit,  $S_1$ . Then by turning either  $M_1$  or  $M_2$  so that the beam fell outside the test cell,  $L_1$  was moved so that the image of the point was a minimum at the premeasured distance. Corrections were not made for a very slight distortion caused by the quartz windows because the point of the beam crossover was predetermined geometrically.

### 3.4.2 Beam Balance

The actual balancing of the two beams was achieved by either varying an aperture in one of the arms or by adding neutral density filters. The former method causes a change in the relative distribution over the elements of the optical path. The latter is limited because of the cutoff of the glass substrates at about 3900 Å. By using quartz, this limit can be

moved down to  $< 2000 \text{ \AA}$ . This transmission characteristic causes a variation in intensity over the entire recorded spectrum. The net result is an intensity match only at the monitored wavelength. This nullifies to some extent the advantage of the photographic methods, that of simultaneously obtaining a large quantity of information. This problem can be eliminated through the choice of a beam splitter and the elimination of other nonsymmetric frequency-dependent attenuators such as extraneous coating on optics. For example, the quartz viewing ports became heavily coated with various copper compounds after several hours of arc running which cause preferential attenuation.

### 3.5 MICROPHOTOMETER

The recording microphotometer is designed for precision measurement of the blackening of photographic emulsion. It magnifies by 15X the image of the plate utilizing a high illumination source. As a photographic plate is scanned the images of the spectral lines move across a slit; the intensity of the images is proportional to the light transmitted by the plate. Thus the current output of its photomultiplier is proportional to the transmission coefficient of the line. The current is amplified and used to drive a strip-chart recorder. The microphotometer is capable of speeds as low as 0.5 mm/min or 0.25 A/min.

The carriage motion was insufficiently reproducible over long distances on the plate because of motor and gear slack. Measurements taken from the microphotometer yielded essentially the same results as those of the contour projector (3.6 below); however, many more passes were required to approach the same level of confidence.

### 3.6 CONTOUR PROJECTOR

A contour projector was also used to read displacements from photographic plates. Measurements to 0.0001 in. can be made (which corresponds to  $0.0127 \text{ \AA}$ ). The projector allowed manual reading of carriage displacements as viewed from a projection screen. Magnifications from 10X to 100X were possible, and the lowest possible magnification compatible with measurement accuracy was used. The contour projector was most satisfactory, especially since it permitted human judgment which was not inherent in the microphotometer.

## SECTION IV PHOTOELECTRIC SCANNING

The equipment required for the method is shown in the block diagram (Fig. 13). Light from the spectrometer was scanned across a 10- $\mu$  exit slit onto the photomultiplier tube. This was in turn amplified and filtered before entering the oscilloscope. Display synchronization was obtained through a trigger circuit. Certain optional components are indicated but were not utilized.

### 4.1 REFRACTOR PLATE

The scanning was accomplished by means of a rotating refractor plate located in front of the exit slit. A small d-c motor was used to turn the refractor plate at speeds as low as 2 rpm (Fig. 14). Also shown in the photo is the microswitch and cam which, through a filter circuit, triggered the oscilloscope. A leaf spring was added (not shown) which applied pressure against the cam collar, reducing backlash in the gear train. The amount of displacement of the light rays for a given angular displacement was assumed to be linear for near-normal incidence.

### 4.2 ELECTRONICS

Figure 15 shows the electronics schematic. The photomultiplier tube (10-mm-diam photocathode) was supplied by a 2000-V dc power supply. The signal from the photomultiplier tube passes through an input filter consisting of a 1-M $\Omega$  resistor in series and a 0.002  $\mu$ f capacitor in parallel for noise elimination. The filtered signal then enters a variable bandpass filter preamplifier plug-in unit (response from 0 to 100 Hz) where further noise elimination takes place. The signal is then displayed on the oscilloscope where a conventional scope camera was used.

The triggering unit removes voltage pulses attributable to switch chatter, eliminating false triggering. There is no negative pulse upon release of the switch because of the delay constant of the low pass section (0.06 sec). The high pass section does not respond to this

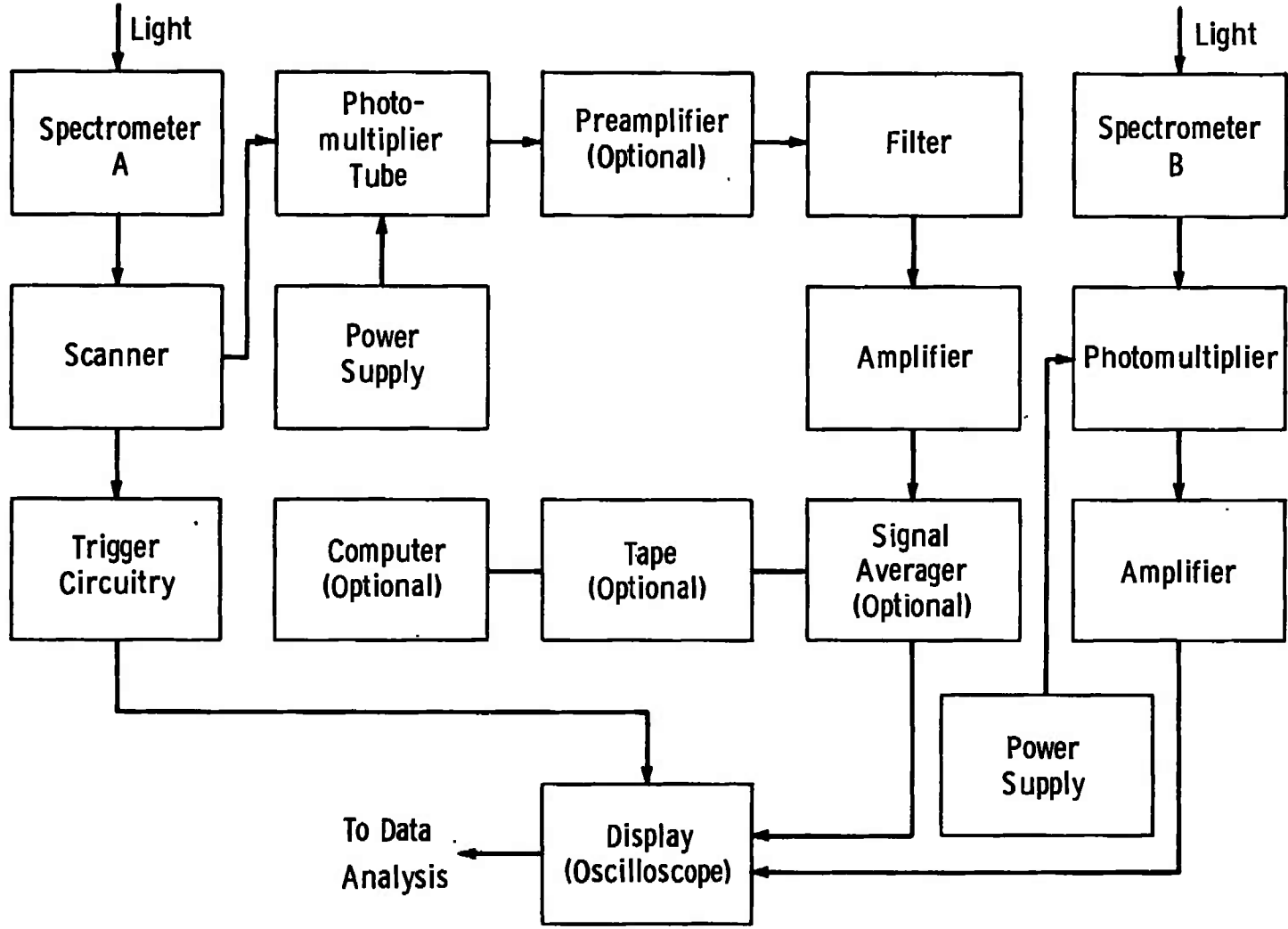


Fig. 13 Photoelectric Scanning

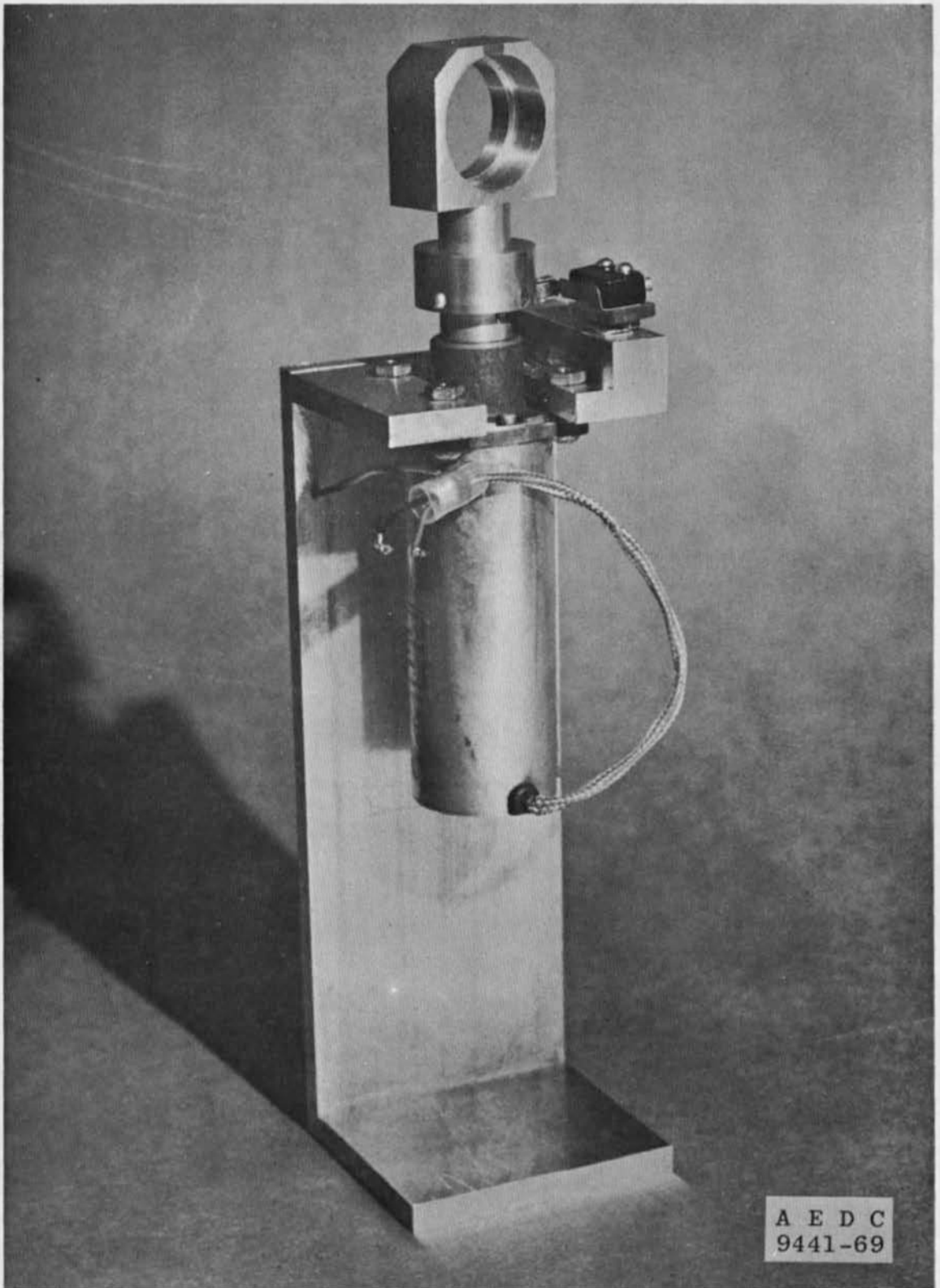


Fig. 14 Refractor Plate

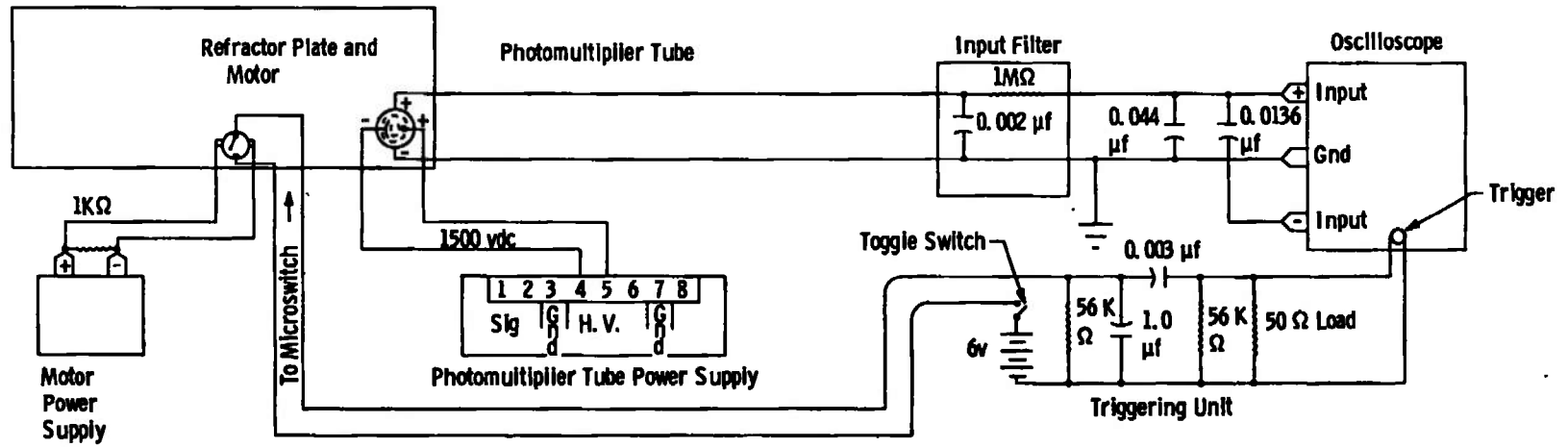


Fig. 15 Electronics Schematic

delay. Variations in  $C_2$  and  $R_2$  can be made to match input impedance if it is not  $50 \Omega$ . With a  $50 \Omega$  load,  $R_2$  was not required.

## SECTION V DATA ACQUISITION

After the intermediate optics and spectrometer were aligned, a prerun check was made. With the photoelectric equipment in place and with the scanner running at a nominal 2 rpm, the two Fe lines, 4271.16 and 4271.76 Å, were observed for a calibration, intensity, and focus check. Also, if the signal-to-noise ratio was poor, corrective steps were taken. The arc was then started and allowed to stabilize. During this time the Ar II line to be used was located and appropriately centered on the oscilloscope. This was achieved with the aid of the grating angle adjustment.

### 5.1 INTENSITY MONITOR

Variations in the intensity level of the two lines over an extended series of shots resulted in data which were considered unsuitable for use with the Abel inversion program. Therefore, a monitoring system was arranged and tested. It consisted of a 0.25-m spectrometer and associated optics. It viewed the same axial station as did beams 1 and 2. Its output was placed on a dual-beam oscilloscope so that a monitor level and signal trace were recorded simultaneously. After the data were analyzed, the level was used to normalize the line profiles. The results of this study indicated a variation of less than 7 percent while data were being obtained. Corrections based on this monitor system did not improve the data. However, it cannot be said that such a technique, especially if used as an automatic gain control, would not contribute substantially to the accuracy of the Abel data.

For general application, however, a line intensity-time profile is desirable, especially if the time of measurement is on the order of the time required for a nominal 5 percent level change to occur.

### 5.2 PHOTOGRAPHIC DATA ACQUISITION

The type of photographic plate used to record the data was a compromise between resolution, run time, and wavelength response.

The 103F plate had good sensitivity from the ultraviolet up to about 5700 Å with medium grain size and medium contrast. The slower speed SAI plates had a cutoff of about 4300 Å, with fine grain, medium contrast, and higher resolution. Because of the optics cutoff wavelength (3900 to 2000 Å), below which the light was readily attenuated, the range of available wavelength was limited to not much more than 4200 to 4300 Å for glass or 2000 to 4300 Å for quartz with the SAI plate. The corresponding ranges for the 103F plate were greater—3900 to 5700 Å for glass and 2000 to 5700 Å for quartz optics.

Exposure times for the 103F using a 20- $\mu$  entrance slit were 0.5 to 5 sec for the argon lines and 15 to 40 sec for the iron arc source medium to strong lines.

Background fogging was found to be high if the plates were not warmed from cold storage temperatures before use.

Exposures taken over extended periods of time required dimensional stability of the plate and camera assembly, which required an elaborate method of spectrometer isolation.

Data were taken in the manner indicated in Table I. Each run consists of various combinations of the radiation taken from either the upper stream, downstream arc source or the iron arc standard. Rack positions correspond to different run numbers and to different exposure bands on the plate.

## SECTION VI DATA REDUCTION

Data reduction methods were largely a function of the method of acquisition. The photoelectric data could be directly reduced by means of the peak displacement method. Also, if a composite were taken, the  $\alpha$ ,  $\beta$ , and  $\gamma$  (or line shape) methods could be applied. For the photographic plate method, the photographic plate first had to be developed, then the data were either reduced to an intensity trace by means of a photodensitometer, or relative displacements were measured by the contour projector. In the case of the photodensitometer method, the  $\alpha$ ,  $\beta$ , and  $\gamma$  methods were applicable.

### 6.1 PHOTOELECTRIC REDUCTION

Electronic data, when taken as a photograph of the oscilloscope trace, were immediately ready for data reduction. Peak-to-peak

**TABLE I**  
**PHOTOGRAPHIC PLATE IDENTIFICATION**

Run No.	Rack No.	Time, Sec	Beam Direction, Source*	Slit Height, mm	Slit Width, $\mu$
1	300	5	1, Ar II	3 ↓	20 ↓
2	350	5	2, Ar II		
3	400	2.5	1 and 2, Ar II		
4	500	5	1, Ar II		
		15	Fe Arc		
5	550	5	2, Ar II		
		15	Fe Arc		
6	600	2.5	1 and 2, Ar II		
		15	Fe Arc		

\*Beam direction (1 or 2) is described by the angles  $\theta_1$  and  $\theta_2$  in Fig. 1.

Plate Type: 103F Emulsion

Grating Angle: 14.00 deg

Date: 1/1/70

Data Point Number: 200

measurements were made directly from the traces as shown in Fig. 16. When noise was a factor, several estimates of peak  $\lambda$  were made by graphically deriving the half-width of the envelope at selected fractional values of  $I_0$ . Unless one of the lines was badly skewed by reflections of oppositely shifted radiation within the test cell (corner reflection) displacements obtained in this manner agreed with direct peak measurements. Calibration was obtained by simultaneously scanning the iron lines, which are separated by 0.605 Å (Fig. 17). This is not the only possible method for obtaining the dispersion. An iron line and even a shifted Ar II could have been used if

$$\left| \frac{\lambda_D}{\lambda_{Fe} - \lambda_{Ar}} \right| \ll 1$$

For most lines this criterion is easily met. The average shift was  $0.0608 \pm 0.0063$  Å with a resolution of 0.103 Å. For the viewing angles of 64.1 deg, this corresponds to a velocity of  $4340 \pm 474$  km/sec.

As a check, the  $\alpha$ ,  $\beta$ , and  $\gamma$  methods were used to determine their reproducibility and limitations because of the approximations used. For all these methods a base line was drawn which approximately averaged out the noise level. As a reasonable curve fit was obtained, the Doppler shift values based on the Gaussian curve were used. Mismatches in intensity were averaged whenever two measurements of the same quantity could be obtained for a single variable; e. g., when the  $\gamma$  method is used, two measurements of the two single line half-widths could be averaged. The results are tabulated in Table II.

## 6.2 PHOTOGRAPHIC REDUCTION

The microdensitometer comparator with a strip-chart recorder output was used originally to obtain a trace of the line profiles. Although the accuracy of the instrument was adequate for intensity studies, a wavelength error of  $\pm 0.025$  Å/in. was not sufficiently small to measure differences from 0.02 to 0.07 Å. Measurements were made using this device, but a large quantity of redundant densitometer tracings were required for each line and are not included here.

Data tabulated in Table III were taken with the contour projector. All measurements were taken relative to fixed Fe lines, but were numerically compared to the composite Ar II line. This artifice served no purpose other than to indicate mismatches in intensity. The net shift is, therefore, the algebraic sum of these differences.

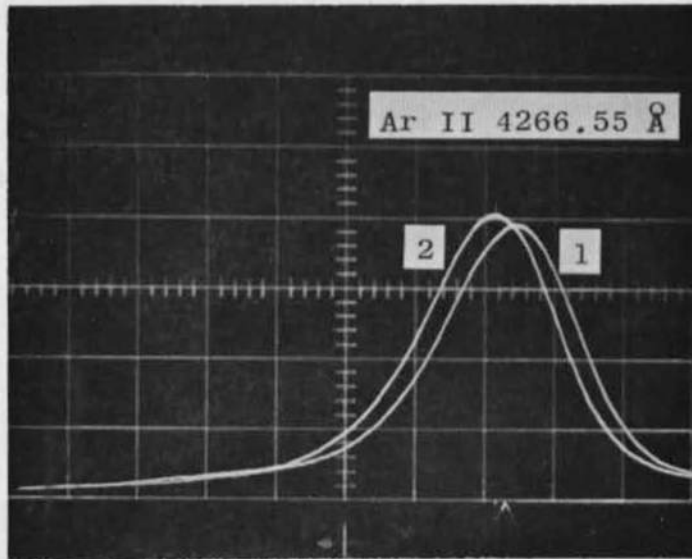


Fig. 16 Shifted Argon Lines

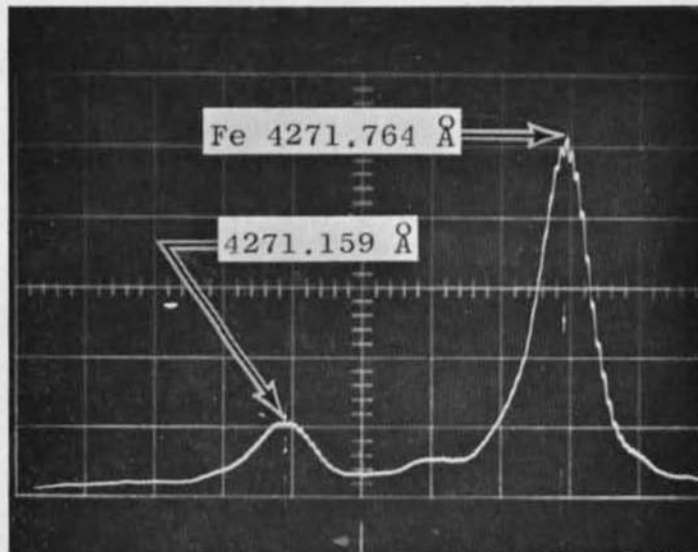


Fig. 17 Iron Calibration Lines

**TABLE II  
TEST RESULTS OF PHOTOELECTRIC TECHNIQUE**

Wavelength 4266 Å

Peak-to-Peak $\Delta\lambda_D, \text{Å}$	Reduction Method			
	$\alpha$ $\Delta\lambda_D, \text{Å}$	$\beta$ $\Delta\lambda_D$	$\gamma$ $\Delta\lambda_D$	
0.0579	0.0958	0.0614	0.0211	
0.0579	0.0896	0.0806	0.0719	
0.0527	0.0780	0.0850	0.0795	
0.0754	0.0186	0.0680	0.0675	
0.0560	0.0654	0.0720	0.0763	
0.0615	0.0834	0.0673	0.0930	
0.0560		0.0630	0.0763	
0.0527		0.0707	0.0682	
0.0670		0.0544	0.0598	
0.0688		0.0755	0.0759	
0.0688		0.0783	0.0773	
0.0600		0.0695	0.0744	
0.0670		0.0581	0.0554	
0.0583		0.0666	0.0765	
0.0565				
0.0565				
<b>Average</b>	<b>0.0608 ± 0.0066</b>	<b>0.0718</b>	<b>0.0693</b>	<b>0.0695</b>
$\bar{V}$	4340 ± 474	5140 ± 2010	4960 ± 400	4970 ± 1180

**TABLE III**  
**TEST RESULTS OF PHOTOGRAPHIC TECHNIQUE**

Wavelength ( $\lambda_0$ ), Å	$\Delta\lambda_D$ , Å	$(\Delta\lambda_D)/\lambda_0 \times 10^6$
4426	0.020	4.53
4228	0.111	25.9
4228	0.046	10.7
4228	0.071	16.5
4013	0.039	9.4
4013	0.023	5.7
4013	0.076	18.75
3928	0.113	27.8
3850	0.050	13.0
3850	0.091	23.6
3850	0.067	17.4
3765	0.040	10.65
3765	0.080	21.3
3729	0.087	23.2
3729	0.036	9.65
3588	0.067	17.25
3588	0.045	12.55
3576	0.073	20.4
3576	0.017	12.8
Average:		15.84 ± 6.72
Velocity:		5400 ± 2310 m/sec 1σ on mean 530 m/sec

### 6.3 ABEL INVERSION

The results of the Abel inversion are shown in Figs. 18 and 19. Note that a strong peaking occurs at ring 5. This is believed to be caused by the presence of barrel shocks within the plume itself. As can be readily observed, actual peak location is in question. Several methods were used to determine the peak: (1) determination of the centroid, (2) peak displacement, and (3) a series of midpoint values. None gave very satisfactory results for three reasons. First, the time constant of the system includes a built-in skew in the data, especially in the tails. This had the most effect upon method (1) above. Second, the number of data points did not allow an accurate peak determination. Finally (3), the overall noise level caused oscillations in the inverted data. This is very evident in Fig. 20 which shows the propagation of error radially inward.

## SECTION VII SUMMARY

Of the systems utilized, the rotating refractor plate synchronized to the oscilloscope provided the most flexible system. It provided better resolution than photographic techniques because a very small exit slit could be used ( $10 \mu$ ). Whenever time is not a factor, as in the case of continuously running facilities, the refractor plate technique can provide high signal-to-noise data.

One restriction the refractor plate imposed was dead time. Data were only taken over a small portion of the plate revolution, 0.8 sec, and the total time between scans was about 30 sec. A resettable scanner might provide a solution.

The photographic techniques, on the other hand, provided a large number of lines from which to work. When plates are to be exposed for species identification, concentration, or other such spectroscopic studies, very little extra work could provide velocities as well. However, because of the effects of emulsion grain, and the requirement of spanning relatively large distances on a plate to reach a reference line, this method is less precise and generally more time consuming than the other methods.

Of the data reduction methods described, the more straightforward methods of measurement and peak displacement proved to be the most accurate as well as requiring the least number of data points. The line

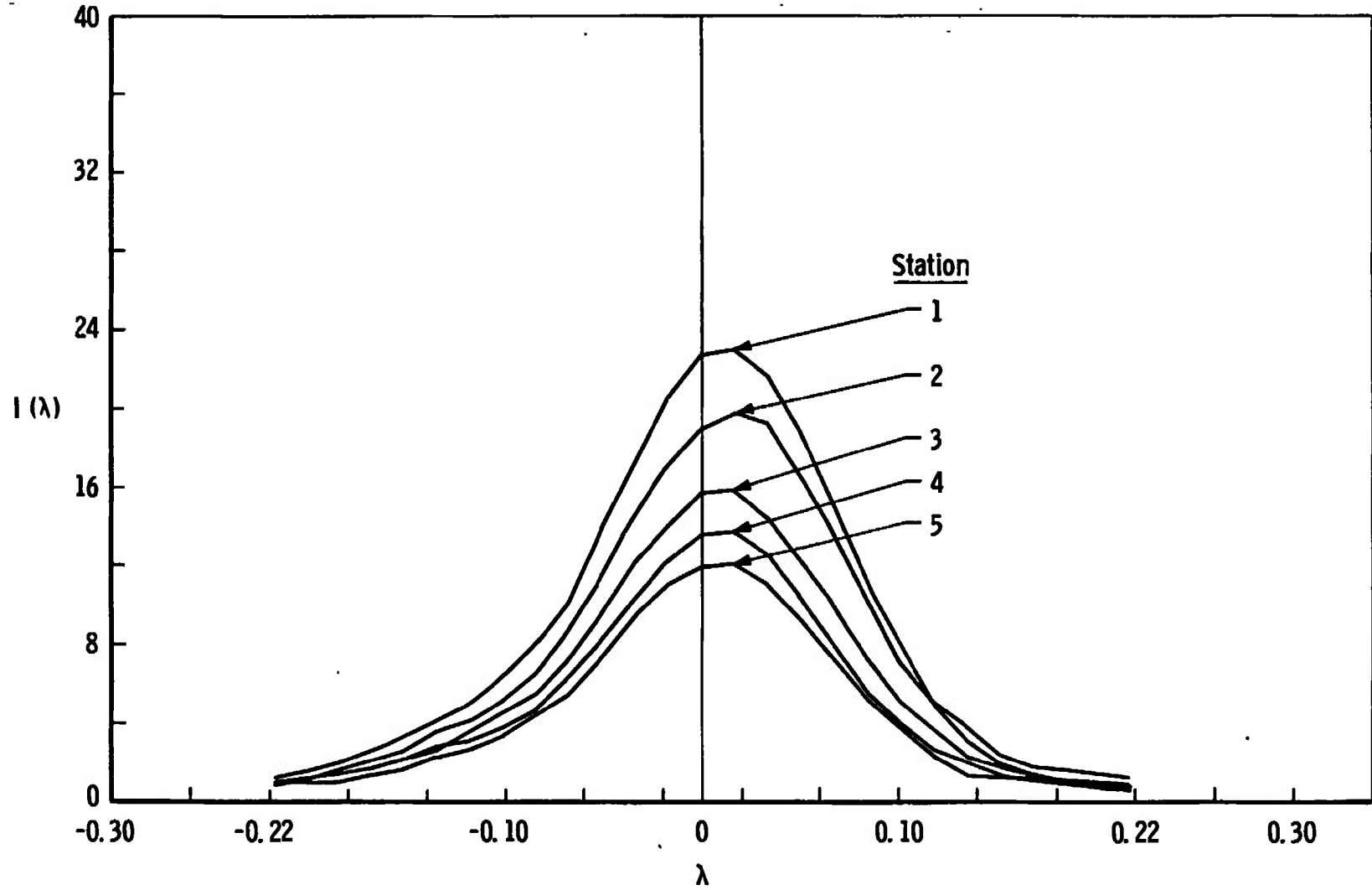


Fig. 18 Abel Inversion with Intensity Monitor, Input Data

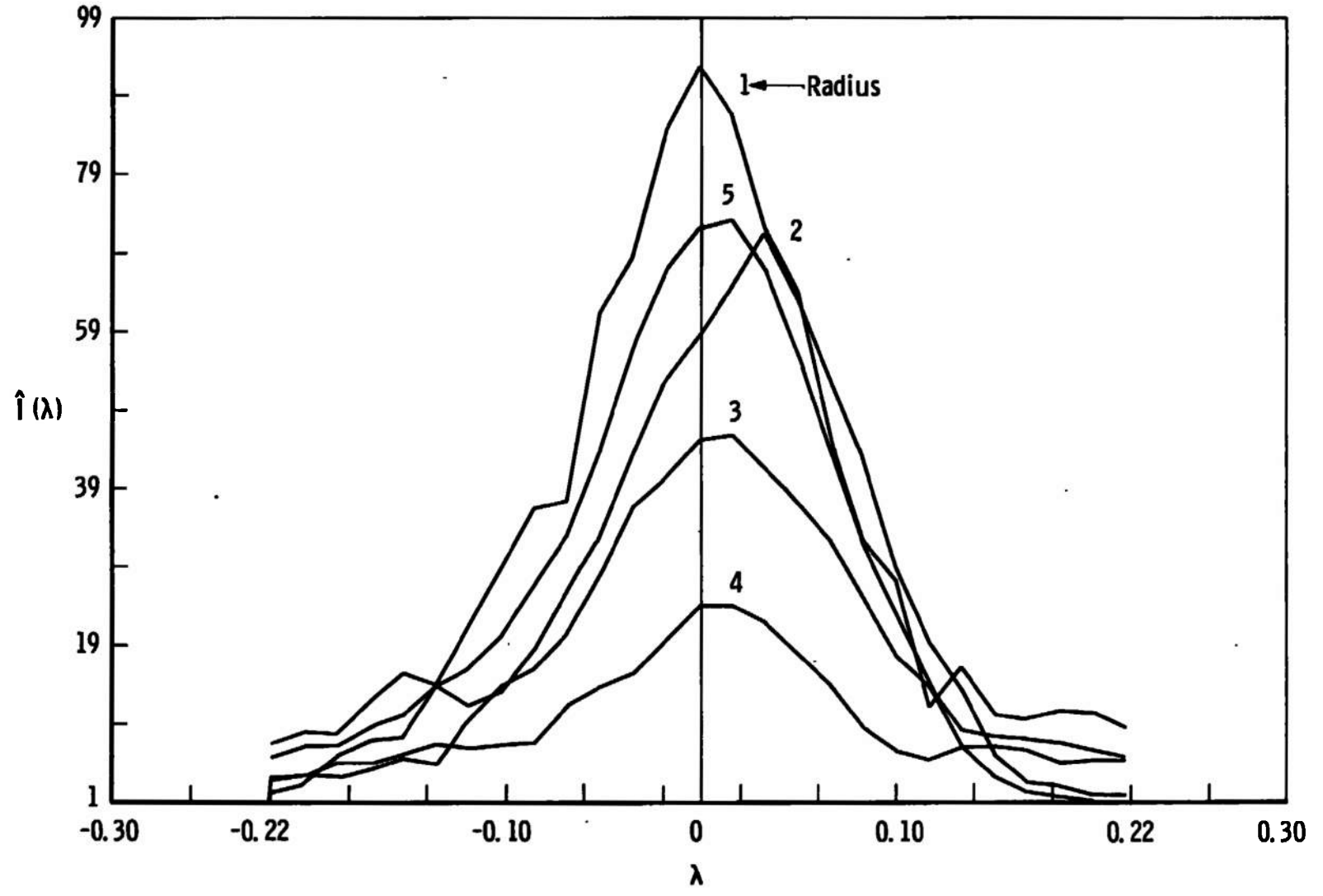


Fig. 19 Abel Inversion with Intensity Monitor, Inverted Data

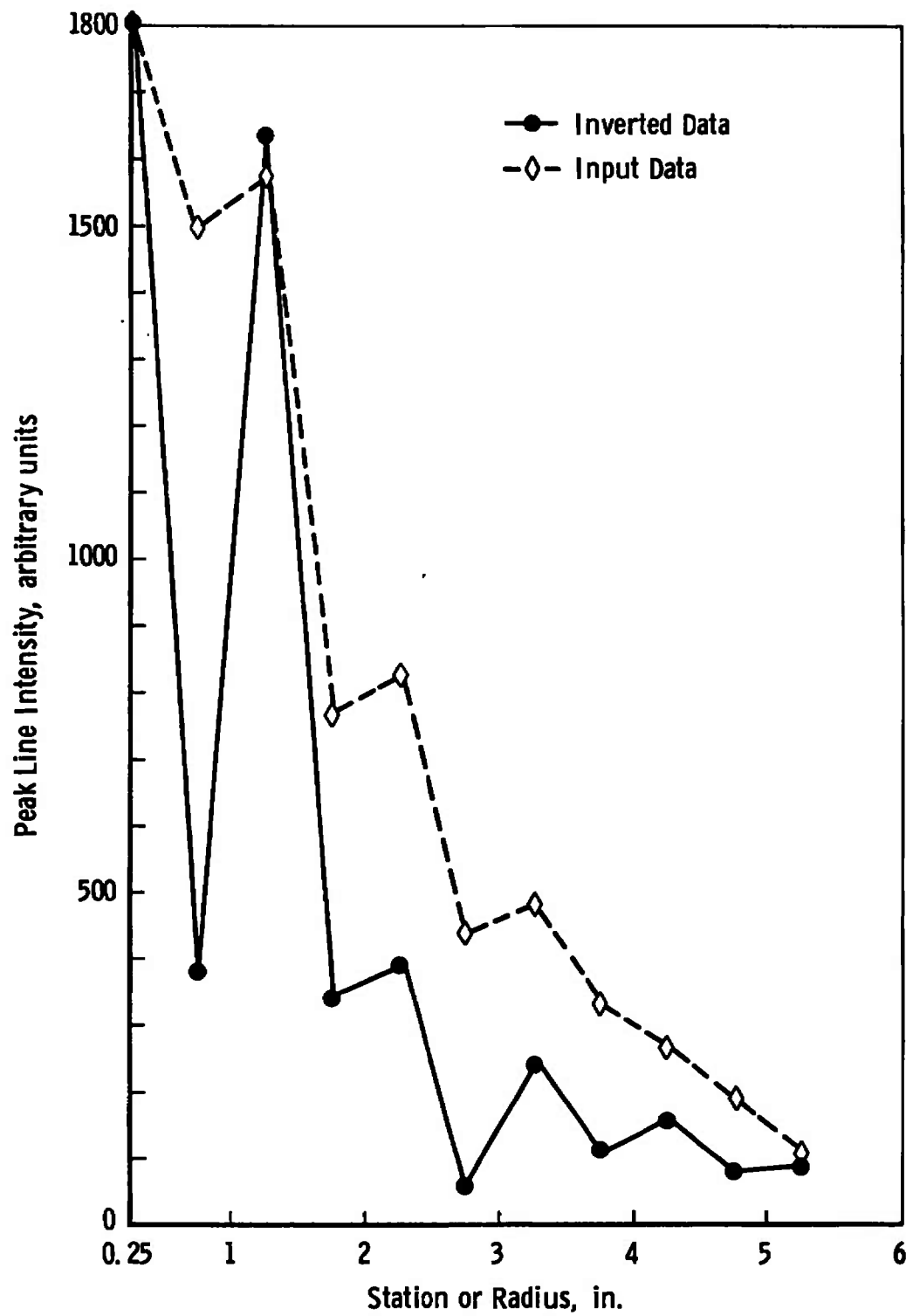


Fig. 20 Comparison of Input and Inverted Data at Peak Intensities

shape methods gave fair agreement with the peak displacement methods but usually suffered from improper choice of base line or non-Gaussian effects.

Application of an Abel inversion should follow (1) an increase in the signal-to-noise ratio and (2) a study of the instrumental broadening effects on the observed lines. Methods presently exist to eliminate instrumental effects from special classes of line shapes (Ref. 6). Much of the inaccuracy associated with the inversion is attributable to manual data manipulation; early conversion of the data to a form more easily handled by a digital computer would benefit the system.

### REFERENCES

1. Maecker, H. "Plasma Streaming in Arcs Caused by Self-Magnetic Compression." Z. Physik, Vol. 141, No. 1-2, 1955, pp. 198-216.
2. Kogelschatz, Ulrich. "Doppler Shift Measurements of Axial and Rotational Velocities in an MPD Arc." AIAA Paper No. 69-110, January 1969.
3. Bohn, W. L., Beth, M. -U. and Nedder, G. "On Spectroscopic Measurements of Velocity Profiles and Non-Equilibrium Radial Temperature in an Argon Plasma Jet." Journal of Quantitative Spectroscopy and Radiative Transfer, Vol. 7, No. 4, pp. 661-676.
4. Ahlborn, B and Morris, R. N. "Plasma Velocity Measurements by Abel - Unfolding of Doppler Shifts." Journal of Quantitative Spectroscopy and Radiative Transfer, Vol. 9, pp. 1519-1525.
5. Beth, M. -U. and Kling, M. G. "Spectroscopically Measured Velocity Profiles of an MPD Arcjet." AIAA Journal, Vol. 7, No. 11, November 1969, p. 2181.
6. Van de Hulst and Reesink, J. J. M. "Line Breadths and Voigt Profiles." Astrophysical Journal, Vol. 106, July 1947, pp. 121-127.

APPENDIX  
COMPUTERIZED FORM OF ABEL INVERSION

```

FORTRAN IV G LEVEL 18          RADINV          DATE = 70355          15/34/53

0001      SUBROUTINE RADINV(N,C,F)
0002      DIMENSION U(1),F(1)
0003      DIMENSION A(25,25),A1(1),A2(2),A3(3),A4(4),A5(5),A6(6),A7(7),
          *A8(8),A9(9),A10(10),A11(11),A12(12),A13(13),A14(14),A15(15),
          *A16(16),A17(17),A18(18),A19(19),A20(20),A21(21),A22(22),A23(23),
          *A24(24),A25(25)
0004      EQUIVALENCE (A(1,1),A1(1)),(A(1,2),A2(1)),(A(1,3),A3(1)),
          *(A(1,4),A4(1)),(A(1,5),A5(1)),(A(1,6),A6(1)),(A(1,7),A7(1)),
          *(A(1,8),A8(1)),(A(1,9),A9(1)),(A(1,10),A10(1)),(A(1,11),A11(1)),
          *(A(1,12),A12(1)),(A(1,13),A13(1)),(A(1,14),A14(1)),(A(1,15),
          *A15(1)),(A(1,16),A16(1)),(A(1,17),A17(1)),(A(1,18),A18(1)),
          *(A(1,19),A19(1)),(A(1,20),A20(1)),(A(1,21),A21(1)),(A(1,22),
          *A22(1)),(A(1,23),A23(1)),(A(1,24),A24(1)),(A(1,25),A25(1))
0005      DATA A1/1.57080/
0006      DATA A2/2.25565,2.45674/
0007      DATA A3/2.06051,2.69599,3.09748/
0008      DATA A4/2.02891,2.23719,3.10298,3.62649/
0009      DATA A5/2.01706,2.13023,2.43399,3.46836,4.08753/
0010      DATA A6/2.01128,2.08348,2.25572,2.62587,3.80085,4.50156/
0011      DATA A7/2.00802,2.05838,2.17189,2.38535,2.80879,4.10745,4.88057/
0012      DATA A8/2.00600,2.04323,2.12445,2.26717,2.51312,2.98257,4.39322,
          *5.23219/
0013      DATA A9/2.00466,2.03334,2.09465,2.19813,2.36390,2.63750,3.14795,
          *4.66179,5.56162/
0014      DATA A10/2.00372,2.02652,2.07457,2.15358,2.27468,2.45988,2.75790,
          *3.30579,4.91590,5.87259/
0015      DATA A11/2.00304,2.02161,2.06035,2.12291,2.21602,2.35192,2.55405,
          *2.67429,3.45690,5.15763,6.16790/
0016      DATA A12/2.00253,2.01795,2.04909,2.10078,2.17499,2.27995,2.42875,
          *2.64631,2.98685,3.60200,5.38861,6.44971/
0017      DATA A13/2.00214,2.01515,2.04195,2.08425,2.14498,2.22899,2.34425,
          *2.50461,2.73622,3.09580,3.74171,5.61016,6.71970/
0018      DATA A14/2.00184,2.01296,2.03579,2.07153,2.12228,2.19131,2.28384,
          *2.40330,2.57923,2.82389,3.20140,3.87655,5.82332,6.97925/
0019      DATA A15/2.00159,2.01122,2.03090,2.06154,2.10464,2.16254,2.23880,
          *2.33892,2.47176,2.65246,2.90938,3.30389,4.00699,6.02899,7.22950/
0020      DATA A16/2.00139,2.00980,2.02695,2.05352,2.09064,2.14000,2.20414,
          *2.28682,2.39384,2.53441,2.72425,2.99277,3.40349,4.13340,6.22790,
          *7.47136/
0021      DATA A17/2.00123,2.00864,2.02372,2.04699,2.07932,2.12196,2.17679,
          *2.24641,2.33500,2.44836,2.59625,2.79479,3.07415,3.50043,4.25614,
          *6.42087,7.70564/
0022      DATA A18/2.00109,2.00768,2.02104,2.04160,2.07002,2.10728,2.15477,
          *2.21446,2.28921,2.38307,2.50234,2.65662,2.86357,3.15365,3.59486,
          *4.37550,6.60783,7.93306/
0023      DATA A19/2.00098,2.00686,2.01879,2.03710,2.06230,2.09516,2.13674,
          *2.18855,2.25266,2.33200,2.43086,2.55568,2.71667,
          *2.93115,3.23137,3.68698,4.49174,6.78985,8.15402/

```

```

FORTRAN IV G LEVEL 18          RADINV          DATE = 70355          15/34/53

0024      DATA A20/2.00058,2.00617,2.01689,2.03329,2.05580,2.08502,2.12178,
* 2.16724,2.22290,2.29111,2.37473,2.47826,2.50833,2.77545,2.99741,
* 3.30740,3.77693,4.60509,6.96113,8.36521/
0025      DATA A21/2.00079,2.00550,2.01526,2.03005,2.05028,2.07644,2.10920,
* 2.14946,2.19042,2.25773,2.32903,2.41727,2.52520,2.66025,2.83324,
* 3.06241,3.38182,3.86486,4.71574,7.14002,8.57900/
0026      DATA A22/2.00072,2.00507,2.01386,2.02726,2.04505,2.06962,2.09852,
* 2.13446,2.17788,2.23006,2.29269,2.36609,2.45951,2.57163,2.71145,
* 2.89006,3.12619,3.45473,3.95069,4.82389,7.30882,8.78378/
0027      DATA A23/2.00066,2.00463,2.01264,2.02484,2.04146,2.06282,2.08936,
* 2.12166,2.16048,2.20682,2.26197,2.32771,2.40641,2.50141,2.61752,
* 2.76192,2.94596,3.18882,3.52621,4.03513,4.92967,7.47383,8.98390/
0028      DATA A24/2.00060,2.00424,2.01158,2.02274,2.03790,2.05736,2.08145,
* 2.11066,2.14560,2.18707,2.23609,2.29402,2.36268,2.44451,2.54293,
* 2.66286,2.81166,3.00095,3.25033,3.59634,4.11768,5.03327,7.63527,
* 9.17965/
0029      DATA A25/2.00056,2.00390,2.01064,2.02089,2.03479,2.05258,2.07456,
* 2.10112,2.13275,2.17012,2.21404,2.26557,2.32612,2.39753,2.48234,
* 2.58403,2.70764,2.86069,3.05506,3.31078,3.66518,4.19865,5.13479,
* 7.79337,9.37132/
0030      FN=N*11
0031      C(N)=FN*(N)/A(N,N)
0032      DO 2 J=2,N
0033      JU=N-J+1
0034      JUI=JD+1
0035      C(JU)=FN*(JUI)
0036      DO 3 K=JUI,N
0037      3 C(JU)=C(JU)-A(JD,K)*C(K)
0038      2 C(JU)=C(JU)/A(JD,JU)
0039      RETURN
0040      END

```

## DOCUMENT CONTROL DATA - R &amp; D

(Security classification of title, body of abstract and indexing annotation must be entered when the overall report is classified)

1. ORIGINATING ACTIVITY (Corporate author) Arnold Engineering Development Center Arnold Air Force Station, Tennessee 37389		2a. REPORT SECURITY CLASSIFICATION UNCLASSIFIED	
		2b. GROUP N/A	
3. REPORT TITLE VELOCITY DETERMINATION BY MEASUREMENT OF THE DOPPLER SHIFT OF A SPECTRAL LINE			
4. DESCRIPTIVE NOTES (Type of report and inclusive dates) Final Report - July 1969 to July 1970			
5. AUTHOR(S) (First name, middle initial, last name) H. T. Bentley, III, V. A. Cline, and E. D. Tidwell, ARO, Inc.			
6. REPORT DATE April 1972		7a. TOTAL NO. OF PAGES 47	7b. NO. OF REFS 6
8a. CONTRACT OR GRANT NO.		9a. ORIGINATOR'S REPORT NUMBER(S) AEDC-TR-71-175	
b. PROJECT NO.		9b. OTHER REPORT NO(S) (Any other numbers that may be assigned this report) ARO-OMD-TR-71-103	
c. Program Element 64719F			
d.			
10. DISTRIBUTION STATEMENT Approved for public release; distribution unlimited.			
11. SUPPLEMENTARY NOTES Available in DDC.		12. SPONSORING MILITARY ACTIVITY Arnold Engineering Development Center, AFSC, Arnold Air Force Station, Tennessee 37389	
13. ABSTRACT Measurement of gas velocity in a high enthalpy, arc-heated facility has usually been inferentially derived. The ability to measure a directly related quantity, the shift in frequency of an emitting spectral line, enables the velocity to be obtained in a noninteracting manner. The theory concerning the line shape and other inversion requirements is discussed. Three mathematical techniques for separating the lines are discussed and examples of each are given. Furthermore, the results of an Abel inversion are obtained. The test apparatus which consists of the high velocity arc source, optics, spectrometer, and either a photographic plate or electro-optical readout is described, and experimental results are presented. Velocity measurements obtained by the various experimental and mathematical techniques are compared as to accuracy, speed, and ease of data reduction.			

14. KEY WORDS	LINK A		LINK B		LINK C	
	ROLE	WT	ROLE	WT	ROLE	WT
speed indicators lasers doppler effect spectral emittance						

A7FC  
Arnold AFB Texas